Remote Sensing of Environment 312 (2024) 114310

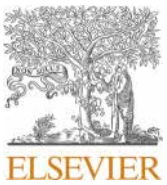

Contents lists available at ScienceDirect

Remote Sensing of Environment

journal homepage: www.elsevier.com/locate/rse

Unoccupied aerial system (UAS) Structure-from-Motion canopy fuel parameters: Multisite area-based modelling across forests in California, USA

Sean Reilly [a,*], Matthew L. Clark [b], Lika Loechler [b], Jack Spillane [b], Melina Kozanitas [c], Paris Krause [d], David Ackerly [c], Lisa Patrick Bentley [d], Imma Oliveras Menor [a,e]

[a] Environmental Change Institute, University of Oxford, Oxford OX1 3QY, UK
[b] Center for Interdisciplinary Geospatial Analysis, Department of Geography, Environment, and Planning, Sonoma State University, Rohnert Park, CA 94928, USA
[c] Departments of Integrative Biology and Environmental Science, Policy, and Management, University of California, Berkeley, CA 94720, USA
[d] Department of Biology, Sonoma State University, Rohnert Park, CA 94928, USA
[e] AMAP (Botanique et Modélisation de l'Architecture des Plantes et des Végétations), CIRAD, CNRS, INRA, IRD, Université de Montpellier, Montpellier, France

ARTICLE INFO

Edited by Marie Weiss

Keywords:
UAS
SfM
Machine learning
Canopy fuels
Biomass
California forests

ABSTRACT

There is a pressing need for well-informed management to reduce wildfire hazard and restore fire's beneficial ecological role in the Mediterranean- and temperate-climate forests of California, USA. These efforts rely upon the accessibility of high spatial and temporal resolution data on biomass and canopy fuel parameters such as canopy base height (CBH), mean canopy height, canopy bulk density (CBD), canopy cover, and leaf area index (LAI). Remote sensing using unoccupied aerial system Structure-from-Motion (UAS-SfM) presents a promising technology for this application due to its accessibility, relatively low cost, and possibility for high temporal cadence. However, to date, this method has not been studied in the complex mosaic of forest types found across California. In this study we examined the capacity of structural and multispectral information obtained from UAS-SfM, in conjunction with machine learning methods, to model aboveground biomass and forest canopy fuel structural parameters using an area-based approach across multiple sites representing a diversity of forest types in California.

Based on correlations with field measurements, fuel parameters separated into vertical (biomass, CBH, and mean height) and horizontal (LAI, CBD, canopy cover) groups. UAS-SfM random forest models performed well for modelling the vertical structure canopy fuels parameters (R^2 0.69–0.75). These models exhibited strong performance in comparison to ALS, as well as when transferred to a novel site. Vertical structure predictors were prominent in these models, and did not improve with the addition of spectral predictors. UAS-SfM random forest models of horizontal structure parameters mainly used raster-based spectral indices (primarily NDVI) and had relatively low performance (R^2 0.49–0.59). In addition, these models underperformed ALS and had poor performance when applied to a novel site. When applied to a region with widespread UAS-SfM coverage, models from both groups successfully produced contiguous maps that could be used for modelling fire behavior or in management decision making and monitoring.

These findings indicate that UAS-SfM, without the need for multispectral sensors, is well suited for mapping area-based vertical-structure canopy parameters across diverse landscapes supporting a wide range of forest types. In contrast, the identification of spectral mean variables for modelling horizontal structure canopy fuels suggests the potential of multi- or hyperspectral sensors or high-resolution satellite imagery for meeting management information needs.

* Corresponding author.
E-mail address: sean.reilly@ouce.ox.ac.uk (S. Reilly).

https://doi.org/10.1016/j.rse.2024.114310
Received 10 November 2023; Received in revised form 28 June 2024; Accepted 3 July 2024
Available online 28 July 2024

1. Introduction

Wildfires shape many ecosystems across the globe, giving rise to highly heterogeneous landscapes due to the spatial and temporal variation inherent in natural wildfire behavior (Beaty and Taylor, 2008; Hessburg et al., 2015; Staver et al., 2011). Fire is a naturally self-limiting process whereby previous burns act as barriers to subsequent fires due to the removal of fuels, defined as biomass available for consumption (Collins et al., 2009; Husari et al., 2006; Keeley et al., 1999; Minnich, 1983; Park et al., 2021; Parks et al., 2015). However, when fire is suppressed or excluded, fuel loads continually rise, eventually surpassing historical levels and eliminating controls on future fire spread or intensity (Prichard et al., 2021; Stephens and Ruth, 2005). As a result of historical suppression practices in the United States, fires now burn at higher severity and on broader scales, despite intensifying suppression efforts (Dennison et al., 2014; Miller et al., 2012; Miller et al., 2009).

Fuel loads in forests of California, USA are a key driver of high-severity fire and are the only parameter governing fire behavior over which managers may exert influence (Duff et al., 2017; Parks et al., 2018). Forest treatments, such as mechanical thinning of the understory, fire breaks, and prescribed fire, can reduce overall fuel quantities and disrupt the spatial continuity of fuels (Agee and Skinner, 2005; Prichard et al., 2021; Stephens and Moghaddas, 2005). To achieve widespread fire hazard mitigation benefits, decision making for treatment optimization and targeting relies upon detailed understanding of fire behavior across the landscape, which, in turn, depends on spatially explicit maps of fuels and/or fuels-related forest structural parameters (Collins et al., 2010; Gale et al., 2021). For example, the initiation of crown torching depends upon vertical forest structural components, such as canopy base height (CBH), while horizontal canopy structural attributes, such as canopy bulk density (CBD) and canopy cover (CC), govern sustained canopy ignition and spread among crowns (Agee and Skinner, 2005; Van Wagner, 1977). Aboveground tree biomass presents an additional parameter of interest for informing treatment selection due to the high imperative for maximizing stable carbon sequestration in the face of climate change (Foster et al., 2020; Hunter and Robles, 2020; Moghaddas et al., 2018).

Measuring these forest attributes presents a significant challenge due to their inherent spatial and temporal variability (Alonso-Rego et al., 2021; Arellano-Pérez et al., 2018). Consequently, remote sensing approaches provide an advantage over traditional field-based manual sampling approaches in that they can estimate continuous fuels parameters over broad extents and are unencumbered by terrain or vegetative barriers to site access. Spaceborne passive sensors generally approximate fuel distributions through the application of fuel density models to observed vegetation classes (Aragoneses and Chuvieco, 2021; Arroyo et al., 2008; Shaik et al., 2022; Stefanidou et al., 2022). These methods are constrained by their reliance on externally-derived fuel models with irregular updates, vegetation maps derived from coarse resolution satellite-based optical imagery, and their inability to account for variation in canopy structure or fuel distribution within a vegetation class, a significant limitation in the structurally-complex forests of California. Alternatively, methods utilizing active sensors, namely airborne laser scanners (ALS) or lidar, provide a means to measure forest structure and fuel loads directly over regional spatial scales (Alonso-Rego et al., 2021; Andersen et al., 2005; García-Cimarras et al., 2021; Hillman et al., 2021b; Kramer et al., 2014; Rocha et al., 2023). However, high cost and equipment requirements of ALS severely limit the capacity of this approach to provide either the spatial coverage or the frequency of repeated measurements required to inform ongoing management of dynamic fuel loads and recurrent fire events at plot to stand scales (Chuvieco et al., 2020; Filippelli et al., 2019; Szpakowski and Jensen, 2019). While lidar mounted on an unoccupied aerial system (UAS) could reduce this barrier, these systems cannot provide spectral data and are not yet sufficiently cost effective to be readily operationalizable in management settings (Gale et al., 2021; Hillman et al., 2021a).

UAS Structure-from-Motion (SfM), the photogrammetric derivation of 3D spatial information from overlapping images, presents a promising technology that could fill this need for readily-acquirable spatial data that directly measures canopy structure and fuel loads at the stand scale (Lowe, 2004; Westoby et al., 2012). The advent of commercial SfM software, coupled with the development of UAS platforms, has significantly reduced the barriers to obtaining and processing highly accurate structural data (Aasen et al., 2018; Adjidjonu and Burgett, 2021; Agüera-Vega et al., 2017; Fraser and Congalton, 2018). At the stand scale, the relatively low cost and ease of imagery acquisition make UAS-SfM well suited for mapping dynamic ecological forces like fuel load accumulation and interannual wildfire events (Chamberlain et al., 2021), as well as effects of management activities (e.g., prescribed burns, thinning). This method has been successfully employed in a variety of ecological applications that measure vegetation structure (e.g., Fu et al., 2021; Navarro et al., 2020; Swayze et al., 2021), including aspects of fire ecology and management (Szpakowski and Jensen, 2019). When coupled with the appropriate sensor, the capacity of UAS-SfM to collect coincidental multispectral data provides additional capability in measuring forest structure and health beyond the limits of lidar data or Red-Green-Blue UAS-SfM (e.g., Abdollahnejad and Panagiotidis, 2020; Reilly et al., 2021).

The capacity of UAS-SfM to measure canopy fuel parameters has only received limited investigation to date (e.g., Shin et al., 2018), especially in California forests (e.g., Forbes et al., 2022; Lamping et al., 2021). The majority of previous related research has focused on coniferous forests (e.g., Alonzo et al., 2018; Sun et al., 2023) or plantation sites (e.g., Chandrasekaran et al., 2022) to measure specific canopy parameters. These studies have achieved strong results due to the ease of tree segmentation under these forest conditions. However, current tree segmentation algorithms fail to segregate individual tree crowns when applied to more complex mosaic canopies, such as oak woodlands (e.g., Chávez-Durán et al., 2024). Consequently, there is a large research gap for UAS-SfM methods, such as area-based approaches, that are capable of modelling canopy fuel loads across a wide range of complex forest types without the prerequisite step of tree segmentation.

In our past research in California forests, we found UAS-SfM possesses the capacity to measure upper-canopy structure and to detect the persistent influence of burn severity on ecosystem structure and vegetation recovery (Reilly et al., 2021). However, our and other research has found the passive sensor mainly detects upper-canopy photons, which hampers UAS-SfM's ability to detect subcanopy structure or directly measure key fuel attributes related to internal structure or lower-canopy strata, such as ladder fuels, CBD, or CBH (Forbes et al., 2022; Reilly et al., 2021; Shin et al., 2018). Modelling approaches to estimate stand parameters can overcome these limitations in photogrammetric techniques by leveraging inherent relationships among distinct components of canopy structure (Filippelli et al., 2019). The capability of this approach to meet the aforementioned research gap in fuels mapping particularly needs to be assessed across a broad spectrum of forest types that characterize heterogeneous forestlands like the ones found across California. Consequently, this paper explores the capability of multispectral UAS-SfM and area-based machine learning to model tree aboveground biomass and canopy fuel parameters across a set of study sites containing forest types representative of the diversity found in California.

Specifically, we address the following objectives:

1. Across a diverse range of forest types, evaluate the accuracy of machine learning models produced using UAS-SfM data to estimate tree aboveground biomass and five important canopy fuel structural parameters: mean height, canopy base height (CBH), canopy cover (CC), canopy bulk density (CBD), and leaf area index (LAI).
2. Compare the accuracy of the best modelling technique produced using UAS-SfM data with the same models produced using ALS data, which has deeper canopy penetration.

3. Using the best modelling technique, evaluate model variable selection and importance.
4. Demonstrate the mapping capability of this modelling approach when utilized in conjunction with wide coverage UAS-SfM data.
5. Evaluate the accuracy of machine learning models produced using UAS-SfM data when applied to a novel site.

2. Methods

2.1. Study sites

We collected UAS-SfM and field data at four sites across northern California that span a wide range of ecosystem types. Data were collected in the summer from 2018 through 2021. LaTour Demonstration State Forest covers 3550 ha in the Cascade mountains of Shasta County ranging in elevation from 1150 m to 2050 m (Fig. 1A). The site is in the Cascades ecoregion (Level 3; Shasta County; Griffith et al., 2016), and populated by mixed conifer forests, with white fir (*Abies concolor*) as the most prevalent species especially at higher elevations (Berbach et al., 1995). The site has active stand thinning and some plots had open canopies. We sampled 27 preexisting 0.04-ha circular California Forest Inventory (CFI) plots between 7 July and 17 July 2020. Jackson Demonstration State Forest covers 19,700 ha acres in the Coast Range ecoregion (Mendocino County) ranging in elevation from 24 m to 670 m (Fig. 1B). The site predominantly contains second-growth coast redwood (*Sequoia sempervirens*) and Douglas fir (*Pseudotsuga menziesii*) that are <120 years old with some isolated remaining old-growth groves and residual trees (Eng, 2015). Most plots had dense, closed canopies. We sampled 10 0.04-ha circular CFI plots between 15 June and 2 July 2020 and an additional 17 CFI plots between 8 July and 12 July 2021. Pepperwood Preserve covers 1261 ha in the Central California Foothills and Coastal Mountains ecoregion (Sonoma County) ranging in elevation from 61 m to 475 m elevation. The site is vegetated with a diverse mosaic of species assemblages including Douglas fir forest, oak woodlands, chaparral, and grasslands (Ackerly et al., 2020; Evett et al., 2013). Note that Pepperwood was almost completely burned in the 2017 Tubbs Fire, with a range from low to high severity across the site. We sampled 22 plots between 1 Sept and 15 Oct 2019. These 0.04-ha square plots have been sampled since 2013 as part of a Sentinel plot network at the site, and the ground truth data for this study were taken from summer 2018 field work (Ackerly et al., 2013; Oldfather et al., 2016). The final site, Saddle Mountain Open Space Preserve, covers 390 ha and is 8 km southeast of Pepperwood. The site has a similar vegetation assemblage to its neighboring Pepperwood site. We established and sampled 22 0.04-ha circular plots between 4 August and 9 August 2020. These plots were established within 60-m of the road and collected as paired points in different forest types. Pepperwood and Saddle Mountain have a Mediterranean climate, whereas Latour and Jackson have a climate associated with temperate coniferous forests. For the sites with preexisting networks of plots (CFI for Jackson and LaTour, Sentinel plot network at Pepperwood), we used a stratified random sampling of plots near roads and away from powerlines, with strata determined by a Principal Components Analysis on ALS structure metrics, adding in an additional consideration of Tubbs burn severity for Pepperwood.

Our plot size was dictated by the preexisting sampling network employed by managers and researchers at our sites for their long-term studies. For management applications and understanding of fire behavior, study plot resolution needs to capture fine-scale forest variation and connectivity. Our small plot size of 0.04-ha, therefore, is well suited for mapping the heterogeneity of biomass and fuels across a site as required to address our research aims (Shugart et al., 2010). The data collected from this scale of plot, however, should be understood to represent local conditions, rather than provide representative measurements of the site as a whole.

2.2. Data sources

2.2.1. Field-based measurements

For this study, we collected tree-level measurements of diameter at breast height (DBH), tree height, and lowest live crown for all stems with DBH >10 cm. We measured DBH at 1.37 m above the ground on the uphill side of the trunk. We employed a Laser Technology Impulse 200 LR Rangefinder to determine tree height. Lowest live crown was defined as the height above the ground of the lowest branch supporting live vegetation within 2 m of the next highest branch and was measured with either a tape measure or laser rangefinder, as practical. At Saddle

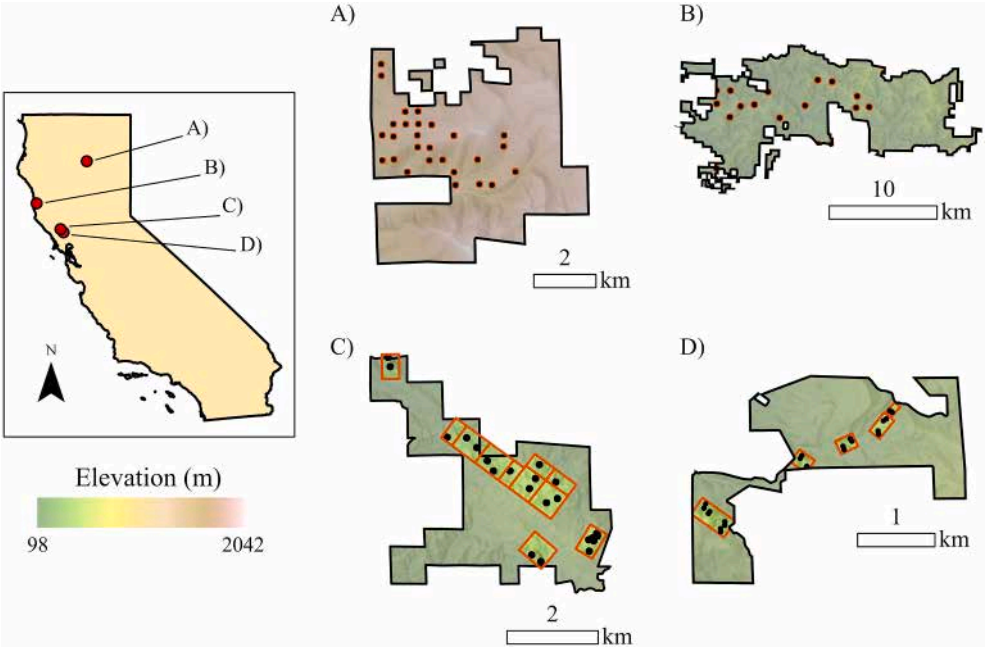

Fig. 1. Map of study sites (a) LaTour, (b) Jackson, (c) Pepperwood, and (d) Saddle Mountain within California, USA. Red boxes denote UAS flight zone perimeters. Black points represent field sites. (For interpretation of the references to colour in this figure legend, the reader is referred to the web version of this article.)

Mountain, we collected all field measurements. At Pepperwood, we utilized DBH measurements previously collected in 2018 as part of the Sentinel site monitoring program. At LaTour, we utilized preexisting DBH and height measurements from a California Department of Forestry and Fire Protection (CAL FIRE) survey conducted in 2020, supplementing as needed with field measurements for plots that had not been included in their campaign. At Jackson, we also utilized preexisting DBH and tree height measurements from CAL FIRE collected in 2020. However, due to the extreme tree height and high canopy cover of the redwood forests at that site, tree heights at Jackson cannot be measured directly. Tree heights, therefore, were estimated from DBH measurements using preexisting CAL FIRE models of the relationship between DBH and tree height (J. Leddy, personal communication, May 17, 2021). We computed individual tree aboveground biomass from DBH and height measurements using the California Air Resource Board's carbon offset protocols based on the U.S. Forest Service's Forest Inventory and Analysis Program volume and biomass equations (FIA, 2014). We took the mean of individual tree measurements for height, aboveground biomass, and lowest live crown to determine plot-level mean height, total aboveground biomass, and canopy base height (CBH), respectively.

We calculated the mean of five measurements per plot (center and 7 m from center in cardinal directions) from the LI-COR LAI-2000 Plant Canopy Analyzer and Forestry Suppliers spherical crown densiometer to measure leaf area index (LAI) and canopy cover, respectively. Canopy cover was estimated in cardinal directions at each of the five locations within the plot, and all cover estimates were averaged for a plot-level measurement. The LAI-2000 uses a handheld wand to measure the percentage of radiation passing through the forest canopy in order to estimate canopy gap fraction and LAI (Keane et al., 2005; Welles and Norman, 1991). LAI-2000 gap fraction measurements were used to compute canopy bulk density (CBD) using the equations from Keane et al. (2005). Keane et al. (2005) conducted destructive sampling at five sites dominated by conifer trees in the western United States to directly measure plot level CBD at varying levels of basal area removal. They modelled the relationship between these measurements and coincidentally collected LAI-2000 measurements as CBD = 0.2231–0.2012 LAI2000A, where LAI2000A represented the mean gap fraction across five zenith angles. This relationship was found to be significant, but with a modest R^2 of 0.56. When using the LAI-2000, we placed one wand in open-canopy areas to measure top-of-canopy radiance, and we strived to take measurements with a second wand within plots during early morning hours to avoid direct sunlight. Both wands had a 45° optic cover with the opening facing away from the sun. The five LAI estimates in a plot were averaged to create one plot-level measurement.

2.2.2. UAS-SfM data collection and processing

This study utilized a MicaSense RedEdge-MX multispectral sensor onboard two UAS platforms. The Micasense sensor detects five spectral bands: blue (475 nm center, 20 nm bandwidth), green (560 nm center, 20 nm bandwidth), red (668 nm center, 10 nm bandwidth), red edge (717 nm center, 10 nm bandwidth), and near-IR (840 nm center, 40 nm bandwidth). At Pepperwood and Saddle Mountain, the sensor was flown using a SenseFly eBee X fixed-wing UAS platform. We flew Pepperwood between September 27 to October 15, 2019 and Saddle Mountain on August 4 and 5, 2020. At Jackson and LaTour, we flew a DJI Matrice 200 (M200) quadcopter UAS platform. We flew Jackson on June 29 to July 2, 2020 and added more sites in July 8–12, 2021. We flew LaTour between July 11 to 16, 2020. UAS platform selection depended upon the availability of a suitable location for fixed-wing take-off and landing. The SenseFly allows for significantly greater mapping coverage per flight but requires a large soft-landing area free from obstructions. The M200 was used in heavily forested sites where these landings were not possible.

Additionally, we used an onboard MicaSense Downwelling Light Sensor (DLS) 2, along with a MicaSense calibration panel (RP04–1926247-OB), for radiometric calibration to convert raw radiance measurements to reflectance values that could be compared between flights across sites. We flew each flight box twice at a flight altitude of 122-m (400 ft) above ground level using a perpendicular crosshatch pattern to ensure maximum coverage. SenseFly's eMotion 3 software (version 3.7) controlled the fixed-wing eBee to collect imagery at 75% latitudinal and longitudinal overlap while the Micasense Atlas app controlled the quadcopter M200 to collect imagery at 85% overlap.

We generated reflectance orthomosaics and SfM 3D point clouds from the collected imagery using Pix4Dmapper (Fig. 2, Pix4D, Lausanne, Switzerland, version 4.4.12). The resulting orthomosaics had 5-cm resolution at LaTour, Jackson, and Saddle Mountain, and 15-cm resolution at Pepperwood. Pepperwood had a lower resolution because of a change in sampling method to prioritize coverage over a larger area. Due to battery flight time restrictions, the eBee had to fly with lower overlap to cover the required area. This resulted in a drop in final orthomosaic resolution when processed through Pix4D. The SfM points clouds had a mean density of 320 points/m^2 with a range from 36 to 672 points/m^2 depending on site characteristics.

We calculated the following spectral indices from the multispectral orthomosaics (Dash et al., 2018):

$$\text{Normalized Difference Vegetation Index (NDVI)} = (\text{NIR}–\text{Red})/(\text{NIR} + \text{Red}).$$

$$\text{Normalized Difference Red Edge (NDRE)} = (\text{NIR}–\text{Red Edge})/(\text{NIR} + \text{Red Edge}).$$

$$\text{Green NDVI (GNDVI)} = (\text{NIR}–\text{Green})/(\text{NIR} + \text{Green}).$$

We calculated these spectral index rasters at the same resolution as the orthomosaic imagery from their respective site (i.e., 5 cm for LaTour, Jackson, and Saddle Mountain, and 15-cm for Pepperwood). These indices were selected based on the available Micasense Rededge MX spectral bands and their relationships with plant physiology (Dash et al., 2018). We then spatially-joined reflectance bands and spectral indices with the point cloud in R (version 4.2.3) using the lidR package (R Core Team, 2023; Roussel et al., 2023). Following the method of Reilly et al. (2021), we identified ground points within the point cloud with a cloth simulation filter and removed erroneously misclassified vegetation points using an NDVI filter (Zhang et al., 2016). We then used these ground points to register the point clouds to preexisting ALS digit terrain models (DTM) (Fig. 2., see section 2.2.3 below). For flight boxes with insufficient identified ground points due to high canopy cover, primarily at Jackson, we performed registration on the complete UAS-SfM and ALS point clouds. Following registration, we height normalized the UAS-SfM point cloud using the ALS DTM and extracted the points within the field plot boundaries.

This study utilized an area-based approach to extracting information from the UAS-SfM data. To summarize these data at the plot level, 216 predictors were generated for modelling inputs (Table 1, Fig. 2). We extracted these predictors directly from the point cloud, rather than from a digital surface model. We computed 40 vertical distribution predictors based on Filippelli et al. (2019) and Marino et al. (2018). These included variables of the height profile, height variation, density bands, and cover. For the density band variables (D_{Hx}), we divided the vertical distribution of points at each plot into ten equal height bands and computed the percentage of points that fell within each of them. For the canopy cover bands, we computed the percentage of points above either 1 m or the mean. Finally, we computed the canopy relief ratio as (mean height – minimum height) / (max height – minimum height) (Marino et al., 2018).

In addition to the vertical distribution predictors, we also generated 176 spectral predictors, divided into raster-based and height-band categories. We generated 16 raster-based spectral predictors by computing the mean and standard deviation from the orthomosaics for the five individual spectral bands (i.e., blue, green, red, red-edge, NIR) and the

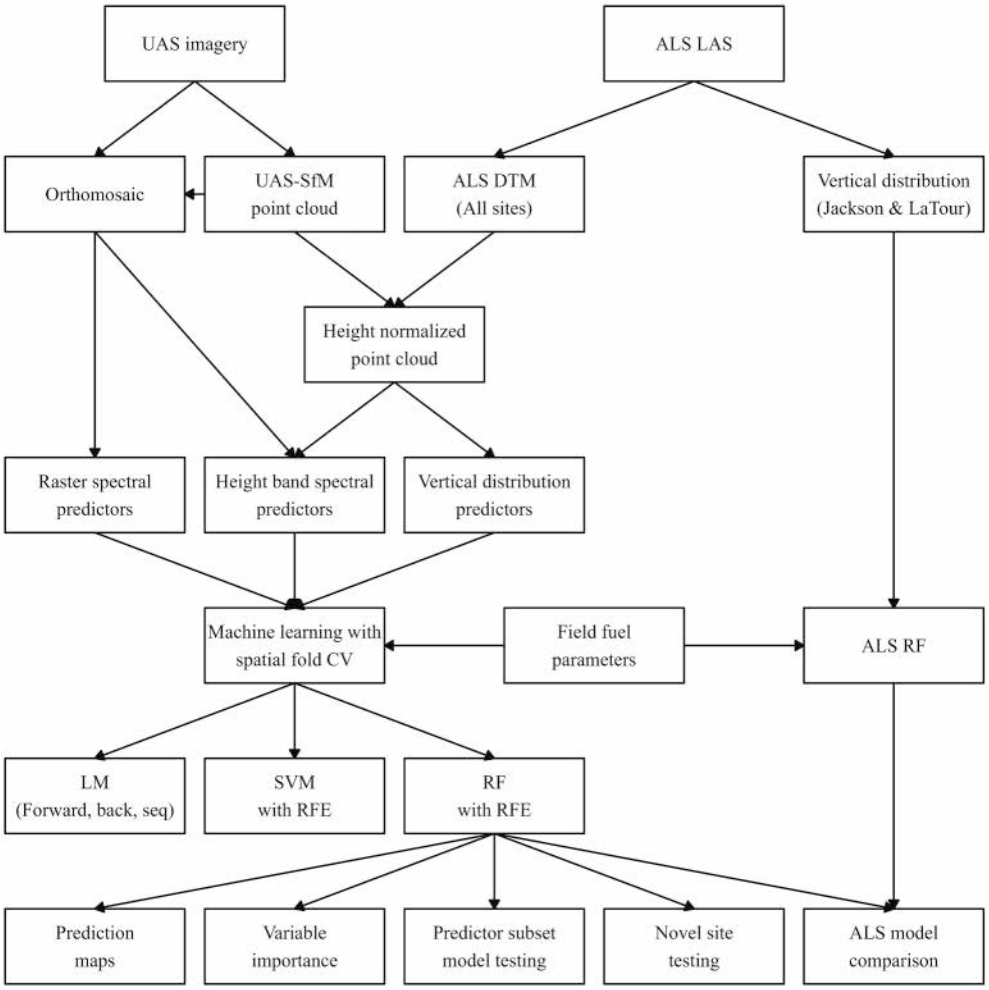

Fig. 2. Data processing workflow.

three spectral indices (i.e., NDVI, GNDVI, NDRE). We also generated an additional 160 height-band spectral predictors. To produce these, we divided the point cloud into ten vertical bins, as we did for the vertical density predictors, and isolated the related spectral information within each bin. For each of these ten slices of the spectral data, we computed the same set of 16 predictors (i.e., mean and standard deviation of the five spectral bands and three indices) to generate 160 height-band spectral predictors in total.

2.2.3. ALS data collection and processing

ALS data for Pepperwood and Saddle Mountain came from the 2013 Sonoma County Vegetation -Mapping and Lidar Program, which were collected by Watershed Science between 28 Sept 2013 and 26 Nov 2013 using aircraft-mounted Leica ALS50 and ALS70 sensors (Watershed Sciences, 2016). ALS data for Jackson were collected by Dewberry and Quantum Spatial between 3 Mar 2017 and 24 Aug 2017 using an aircraft-mounted Leica ALS70 sensor (Dewberry, 2018). ALS data for LaTour were collected by Quantum Spatial between 11 Oct 2019 and 27 Dec 2019 using a Riegl VQ1560i sensor (Quantum Spatial, 2020). Collected ALS data had a mean point density of 25 points/m^2 with a range from 6 to 49 points/m^2. ALS DTMs were generated from ground points within the data as classified following procedures by each company.

We constrained our comparisons between models using both UAS-SfM and ALS data to Jackson and LaTour. The ALS data at these sites were collected within a narrow window of our UAS-SfM campaign and no disturbance events occurred at the sites between collection times. Saddle Mountain and Pepperwood were excluded from this analysis because of the large temporal gap between collection times and a significant disturbance event (the Tubbs fire) that significantly affected the area. Following the UAS-SfM procedure, we height normalized the ALS DTMs and extracted the points that fell within each plot boundary. Since ALS lacks spectral information, only the vertical density subset of variables was computed from these data for modelling input (Fig. 2).

2.3. Machine learning modelling

Following the methods of de Almeida et al. (2019), we tested five regression modelling methods using the caret package in R (Kuhn et al., 2023). Caret, in turn, utilizes a suite of R packages to streamline model training for complex regression and classification algorithms (Cutler, and Original by L.B. and A., Wiener, R. Port by A.L. and M, 2022; Karatzoglou et al., 2023; Miller and Based on F. Code by A, 2020). The models tested in this study comprised three linear models (LM), support vector machine (SVM), and random forest (RF). For each approach, we centered and scaled the predictor variables prior to training the model using caret's default method of subtracting the mean to center and dividing by the standard deviation to scale. Additionally, for the LM methods, we addressed multicollinearity in the predictor set by removing subsets of variables that surpassed a correlation of $r = 0.9$ using the internal caret function.

We assessed model performance using cross validation with spatially-blocked groups. There has been ongoing debate in the literature about the accuracy of spatially-blind cross validation (Ploton et al.,

Table 1
UAS-SfM structural and spectral predictors.

Predictor label	Description	N
Vertical Density		
Z_{max}	Max height	1
$\bar{Z}$	Mean height	1
P_x	Height percentiles in 5% increments (0% to 95%)	20
Z_{SD}	Height standard deviation	1
Z_{CV}	Height coefficient of variation	1
Z_{Kurt}	Height kurtosis	1
Z_{Skew}	Height skewness	1
Z_{IQR}	Height interquartile range	1
CRR	Canopy relief ratio $(\bar{Z} - Z_{min}) / (Z_{max} - Z_{min})$	1
D_{Hx}	Height density bands	10
CC_{1m}	Percentage of points above 1 m	1
CC_{Mean}	Percentage of points above mean	1
Raster-based Spectral		
$\overline{SPECTRA}$	Orthomosaic mean for spectral bands and indices	8
$SPECTRA_{SD}$	Orthomosaic standard deviation for spectra bands and indices	8
Height-band Spectral		
$\overline{SPECTRA}_{Hx}$	Height band mean for spectral bands and indices	80
$SPECTRA_{Hx}SD$	Height band standard deviation for spectral bands and indices	80
	Total	216

Note. Subscript *x* denotes index placeholder for multiple bands. SPECTRA denotes placeholder for individual spectral bands (blue, green, red, red-edge, NIR) and spectral indices (NDVI, GNDVI, NDRE).

2020; Pohjankukka et al., 2017; Wadoux et al., 2021). If neighboring plots are separated into testing and training sets, their inherent spatial autocorrelation could artificially inflate the reported performance of the model. Therefore, we computed a set of spatial variograms for each canopy fuel parameter and used the range of the partial sill as a distance threshold for data splitting (Table 2). The sill range of a spatial variogram is the distance at which the model asymptotically levels out. The partial sill range is the distance at which the model reaches this asymptotic value minus the nugget, the variation in the model due to random or sampling error (Cressie, 1988). This range represents the distance at which spatial autocorrelation has ceased and, therefore, sites farther apart than this distance are appropriate for comparison (Ploton et al., 2020). All sites within this distance threshold comprised a spatially-blocked group that would be collectively assigned to either training or testing subsets at each cross validation split. At each cross validation split, R^2 and RMSE were computed on the held out spatially-blocked group. At the end, the error metrics from all of the cross-validation iterations were summarized into average metrics for the final model. Using this spatial cross validation, each model was optimized using the minimization of the root mean squared error (RMSE) of the fuel parameter predictions.

LM methods seek to establish linear relationships between the predictor variables and given fuel parameter response. LM feature selection occurs in a stepwise manner that can either be done forward, whereby the algorithm starts with an empty model and adds significant variables; backwards, whereby the algorithm starts with a complete model and removes nonsignificant variables; or sequentially, whereby both steps are conducted simultaneously. We tested all three approaches in this study.

SVM is a non-parametric modelling approach that uses a kernel to map predictor variables to higher dimensions in an attempt to generate a linear relationship from nonlinear inputs (Mountrakis et al., 2011; Vapnik, 2006). Based on the results of de Almeida et al. (2019), we employed a radial kernel.

RF is an extension of tree based classifiers whereby an ensemble of individual classification trees generated from bootstrap subsamples of the input data cast votes on a prediction (Breiman, 2001). These models can be tuned by setting the number of randomly selected features per tree split or by selecting the number of trees. A grid search of these tuning parameters found negligible impact on model accuracy.

Prior to final model training, we conducted SVM and RF predictor selection using the Recursive Feature Elimination (RFE) function within caret. This process ranks each feature by importance and sequentially removes them until two remain. It then identifies the lowest number of predictors with an RMSE within the 95% confidence interval of the overall lowest RMSE (de Almeida et al., 2019). We then used this identified subset of predictor variables to train the final models.

For the individual site and ALS model analyses, we followed these same methods. However, due to the small spatial extent and limited sample sizes, we omitted the spatial blocking from the cross-validation process and used a smaller number of cross validation groups. For comparison with UAS-SfM, we modelled canopy fuel parameters with ALS only at Jackson and LaTour as these data were acquired within three years of UAS flights, thereby minimizing differences due to vegetation change in the intervening years. Further, these are conifer-dominated sites with relatively low seasonal variation in leaf phenology.

2.3.1. *Pepperwood area-based mapping*

We applied the final all-site model to a large contiguous region at Pepperwood to demonstrate the capability of this modelling approach, in conjunction with UAS-SfM, to generate continuous maps of canopy parameters as needed for fire behavior modelling and broad-scale evaluation of management practices. Pepperwood was selected for this demonstration because the site's terrain and interspersed grasslands provided adequate landing zones for the eBee fixed-wing drone. This allowed us to collect extensive overlapping flight boxes to generate data over a large region to which the model could be applied (Fig. 1 – Pepperwood).

Vegetation distribution data for Pepperwood was taken from Ackerly et al. (2020). In their study, they utilized a support vector machine (SVM) algorithm to generate maps of land cover classes and tree species distributions from 2-m hyperspectral imagery by the National Aeronautics and Space Administration's Jet Propulsion Lab Airborne Visible Infrared Spectrometer-Next Generation (AVIRIS-NG) on 5 June 2014. We aggregated tree species into three forest types, namely conifer, evergreen broadleaf, and deciduous broadleaf (Reilly et al., 2021).

2.3.2. *Novel site testing*

For the novel site testing, we generated a set of RF fuel parameter models using the data from all sites except for Saddle Mountain using the same methods described above, including spatially-blocked cross validation. We then applied these models to the withheld Saddle Mountain plots to generate a set of test predictions on samples to which the original model had been fully blind. Saddle Mountain was selected for this analysis since the values from Saddle Mountain for all field-based fuels parameters fell within the range defined by the other three sites. All other sites had at least one parameter in which their values exceeded those from the other sites. Since RF models cannot extrapolate beyond the limits of the training data, this would have inherently resulted in poor model performance if the other sites had been withheld and tested in this way.

Table 2
Cross validation spatially-blocked group distance thresholds from spatial variogram partial sill range.

Parameter	Abbreviation	Partial sill range
Biomass	–	44 m
Mean height	–	75 m
Canopy base height	CBH	266 m
Canopy cover	CC	513 m
Canopy bulk density	CBD	487 m
Leaf area index	LAI	103 m

3. Results

3.1. Field-based plot-level aboveground biomass and canopy fuel parameters

The distribution of canopy data measured in the field across sites followed expected patterns based on the dominant species compositions at each site (Fig. 3). Pepperwood, LaTour, and Saddle Mountain generally possessed similar parameter ranges, with Pepperwood consistently belonging to the lowest statistically identified group. In contrast, Jackson, the only site predominantly populated by coastal redwood forests, consistently belonged to the highest value group for all field-based parameters.

Correlation results segregate field-based fuel parameters into two distinct groups which align with the conceptual structural organization of these parameters (Fig. 4). The first group of aboveground biomass, mean height, and CBH are principally vertical measurements of forest structure (biomass allometry leverages height-structure relationships). The second group consists of LAI, CBD, and canopy cover, which are horizontal measures of canopy structure. With the exceptions of the

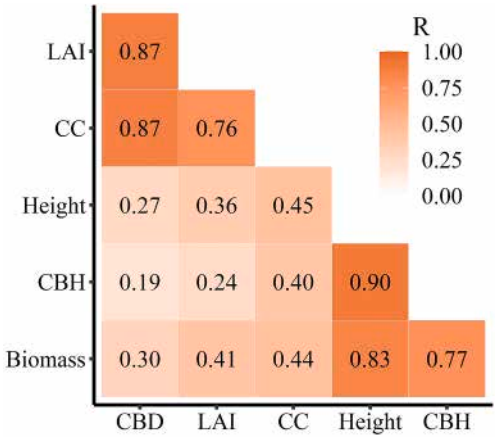

Fig. 4. Field-based plot-level parameter relationships. R values denote Pearson correlation coefficients.

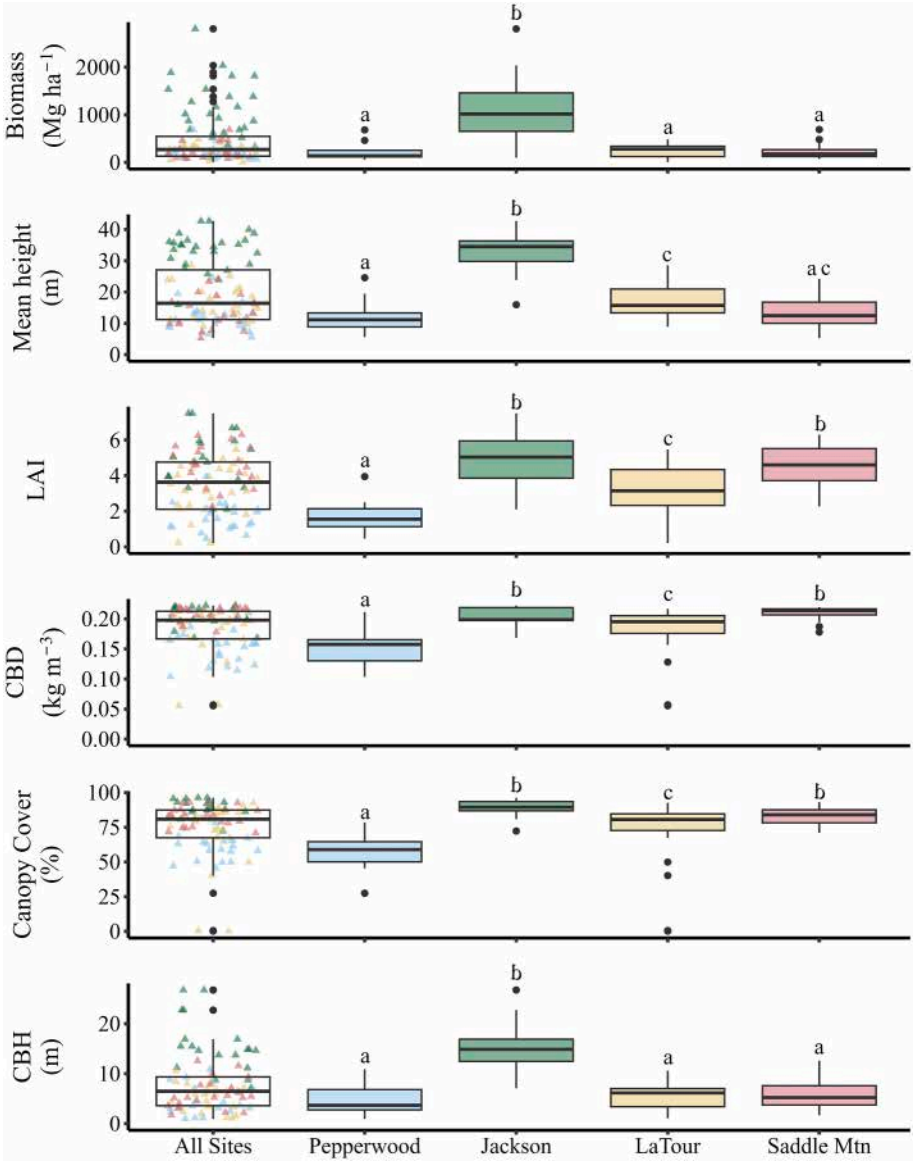

Fig. 3. Field-based plot-level aboveground biomass and canopy fuel parameter estimates across all sites and for each individual site. Lower case letters represent statistically similar groups as determined by ANOVA.

correlations between CBH and CBD ($p = 0.08$) and between CBH and LAI ($p = 0.053$), all correlations between fuel parameters were significant. Correlations within the identified groups were significant at $\alpha < 0.001$.

3.2. Model comparison

While there were significant differences among observed model performances, in general, random forest, SVM, and forward linear regression models explained similar variance in the data for the majority of parameters (Tables 3 & S1). However, across all canopy fuel parameters, random forest did consistently outperform or match the accuracy, as given by R^2 and RMSE, of all other methods (Table 3, Fig. 5). Therefore, the remainder of the analysis in this paper will focus on random forest models. See supplement sections S1 and S2 for further analysis of model comparison and individual site model results.

3.3. Random forest model analysis

Random forest all-sites model performance differed markedly between the vertical and horizontal groups of fuel parameters. The models for the vertical structure fuel parameters of biomass, mean height, and CBH returned R^2 values from 0.69 to 0.75 while the horizontal structure fuel parameters values ranged from 0.40 to 0.59 (Table 3). Apart from canopy cover, the average relationship between predicted versus observed values approximated a one-to-one relationship (Fig. 6). Random forest model error increased markedly for extreme values of each canopy fuel parameter (Fig. 6). We applied the all-sites random forest model to UAS-SfM spatial predictors at Pepperwood to produce estimated fuel loads (Fig. 7). These maps show strong relationships between vegetation classes and canopy fuel parameters (Fig. 7). As expected, coniferous regions demonstrate higher biomass and CBH as compared to broadleaf forest regions (Fig. 7b-c).

Table 3
Models of canopy fuel parameters across all study sites. Mean performance results obtained from 100 replicates of 10 cross validation using spatially-blocked groups. Underlined values denote the statistically most accurate models per canopy parameter as determined by ANOVA at $\alpha = 0.05$ (Table S1). Multiple underlines per row denote statistically equivalent top performance metrics. Mean and standard deviation of all field measurements given as reference for magnitude of RMSE. SVM = Support Vector Machine; RF = Random Forest.

Fuel parameter	Linear methods			SVM	RF	Mean (SD)
	Forward	Sequential	Backwards			
R^2						
Biomass	0.62	0.59	0.56	0.69	0.75	
Mean height	0.72	0.71	0.64	0.71	0.73	
CBH	0.68	0.68	0.63	0.66	0.69	
CC	0.50	0.45	0.41	0.48	0.49	
CBD	0.49	0.48	0.36	0.41	0.50	
LAI	0.38	0.40	0.36	0.45	0.59	
RMSE						
Biomass	12.36	13.00	13.41	11.17	9.28	18.79 (21.04) Mg
Mean height	5.04	5.07	1535.30	5.16	4.85	19.64 (10.22) m
CBH	3.03	2.99	3.27	2.92	2.57	7.69 (5.59) m
CC	12.11	12.91	14.80	11.14	11.17	75.43 (18.61) %
CBD	0.02	0.02	2.27	0.03	0.02	0.19 (0.04) kg m^{-3}
LAI	1.51	35.10	575.9	1.34	1.13	3.54 (1.76)

Height percentiles were consistently in the top five predictors for vertical structure fuel parameter models of biomass, mean height, and CBH (Fig. 8a-c). These predictors capture the vertical distribution of the forest canopy. The model for biomass relied upon a mixture of height percentiles from the lower and upper canopy while the models for both mean height and CBH exclusively utilized height percentiles from the upper canopy.

In contrast, the horizontal structure models of canopy cover, CBD, and LAI had top-five predictors based on spectral indices (Fig. 8d-f). The raster-based mean NDVI emerged as the top variable for all three fuel parameters. The model for canopy cover relied almost exclusively upon this index (Fig. 8d). The model for LAI also exclusively depended upon NDVI, augmenting the raster-based mean with a combination of NDVI height bands (Fig. 8f). The model for CBD supplemented NDVI with other spectral predictors (Fig. 8e). None of these models included individual spectral bands.

See supplement section S3 for SVM and LM variable selection. SVM variable selection closely matched that of random forest and exhibited the same separation between parameter groups. Linear models, in contrast, demonstrated less consistency in variable selection.

Testing the models by isolating predictor variables by data type resulted in distinct patterns between the vertical and horizontal fuel parameter groups (Fig. 9). Restricting the predictors to only the vertical distribution predictor subset resulted in models for the vertical fuel parameters biomass, mean height, and CBH with performance comparable to the model with all predictors, while performance for the spectral-based data subset models lagged significantly behind.

The horizontal parameter group demonstrated much lower variability among models produced with different predictor subsets (Fig. 9). The vertical distribution and raster-based spectral data subset models performed nearly identically for all three fuel parameters. Model performance for both predictor subsets matched that of the full-predictor model for canopy cover but lagged for CBD and LAI. For LAI, only the height band spectral subset model matched the full-predictor model performance, utilizing a set of mean NDVI height bands (Fig. 9, S6). This was the only canopy fuel parameter for which this data subset achieved the maximum accuracy. None of the variable subset models matched that of the CBD full-predictor model. While the performance loss was marginal, all other fuel parameters had at least one variable subset that returned comparable accuracy to the full-predictor model. See supplement section S4 for analysis of predictor subset model variable importance.

3.4. ALS comparison to UAS-SfM data

Apart from the models for biomass at Jackson and LAI at LaTour, ALS-based random forest models outperformed UAS-SfM models across sites and fuel parameters (Fig. 10). ALS performance displayed minimal variation among parameters. Consequently, the difference in accuracy between UAS and ALS was most pronounced for those horizontal structure fuels parameters, namely canopy cover and CBD, which had the largest decrease in UAS-SfM model performance relative to ALS, as compared to the vertical structure parameter group. These differences were particularly pronounced for Jackson, which had dense, closed-canopy coast redwood forests.

3.5. Model testing at novel site

Model accuracy, when transferred to an independent site, differed by fuel parameter group (Table 4, Fig. 11). The vertical parameter group of biomass, mean height, and CBH retained adequate model accuracy at the independent site as compared to the original model cross-validation accuracy. In contrast, the horizontal parameter group experienced significant drops in model performance, and none were well predicted.

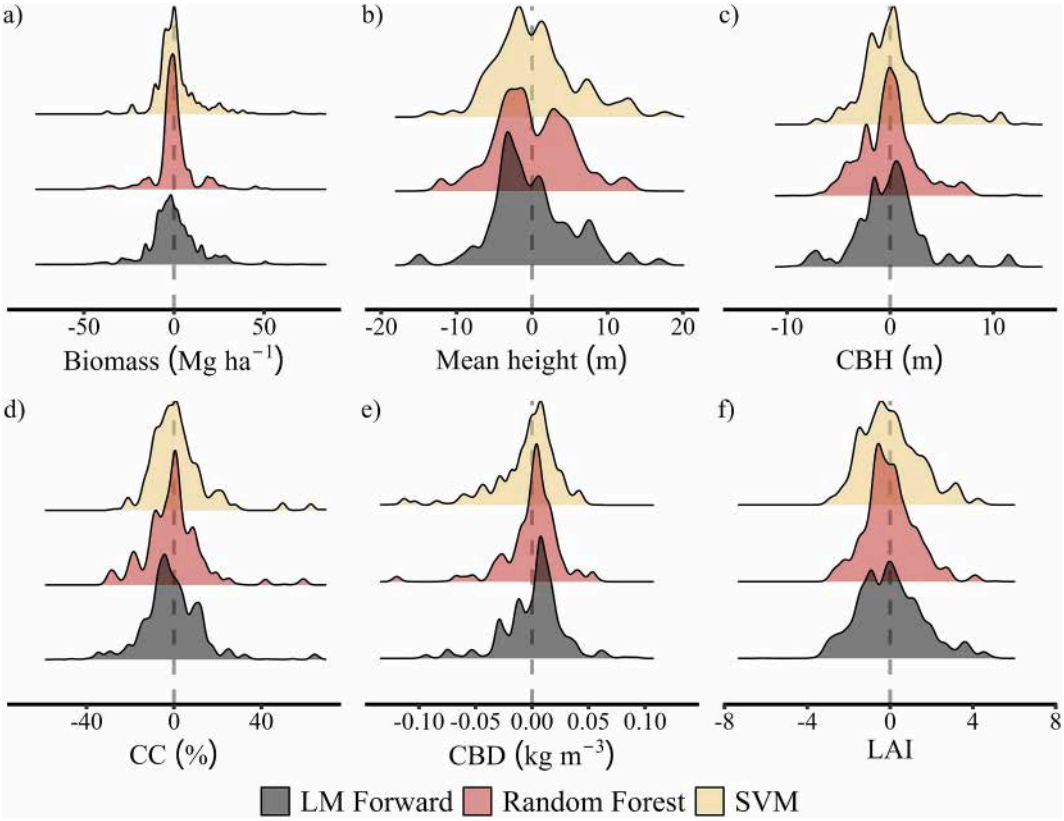

Fig. 5. Model cross validation error density. Individual error measurements taken from 9600 estimates produced across 100 replicates of 10-fold cross validation using spatially-blocked groups.

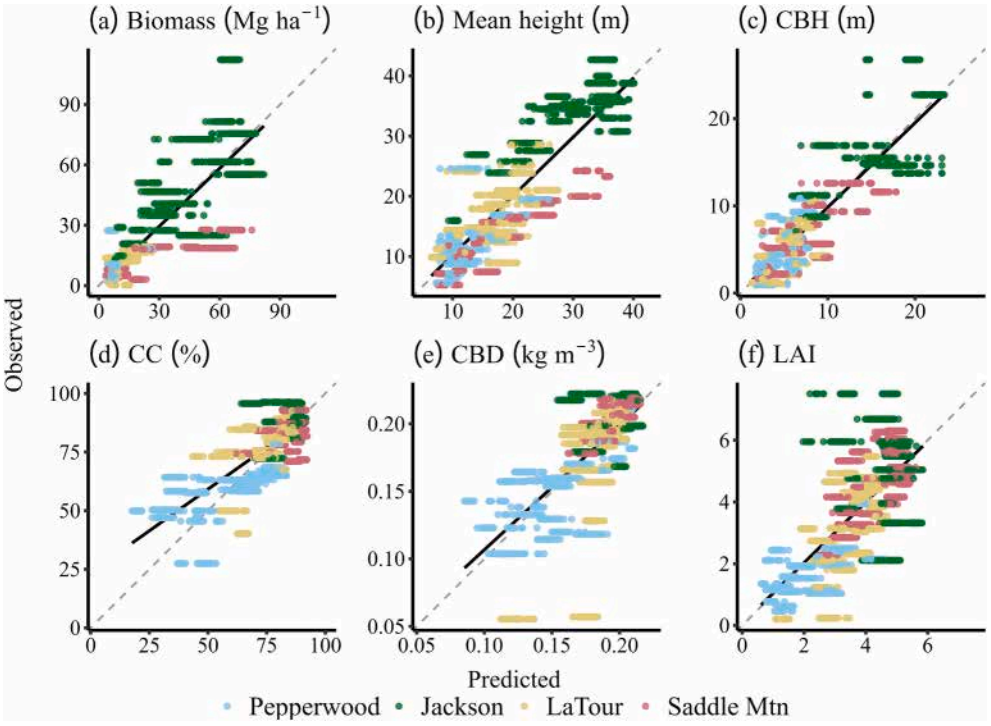

Fig. 6. Random Forest cross-validated predictions versus observed values for all-sites models (Table 3). Grey dashed reference line represents the one-to-one relationship between predicted and observed values. Black solid line denotes the regression best fit.

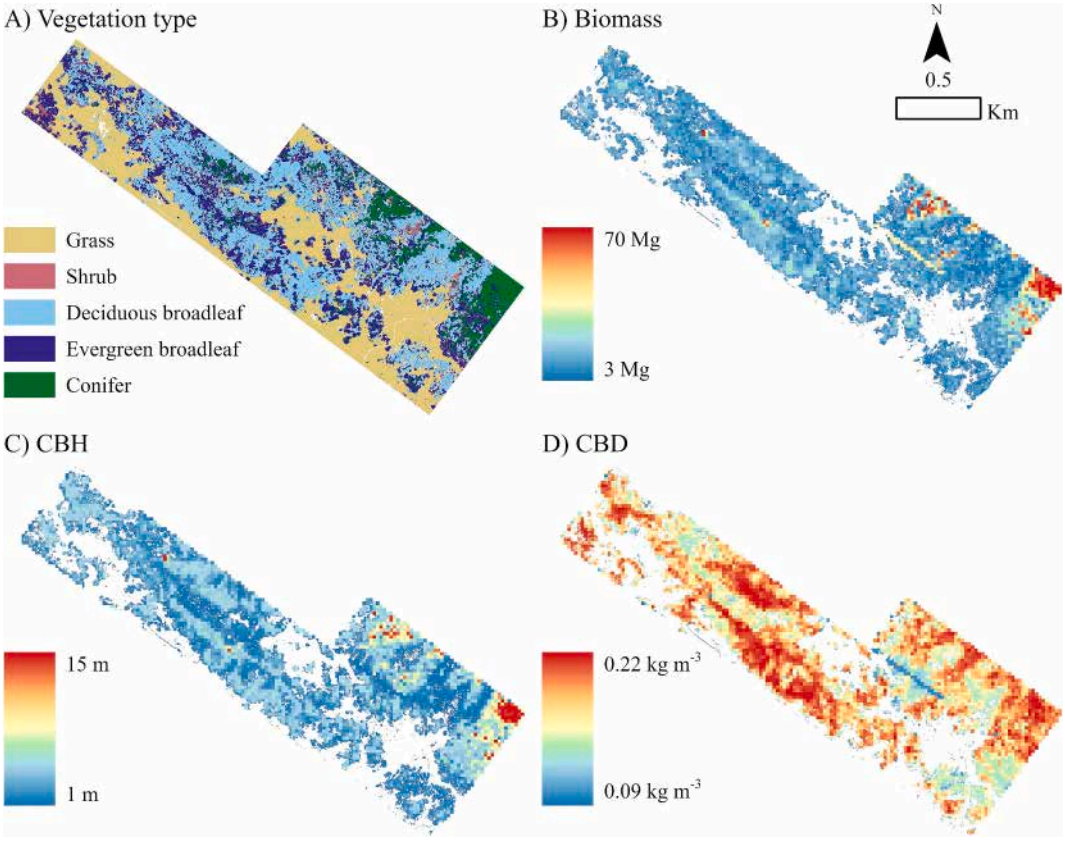

Fig. 7. Pepperwood random forest fuels prediction maps at 20 m resolution from the final all site model for each parameter. White areas are grasslands and shrublands, which were not analyzed.

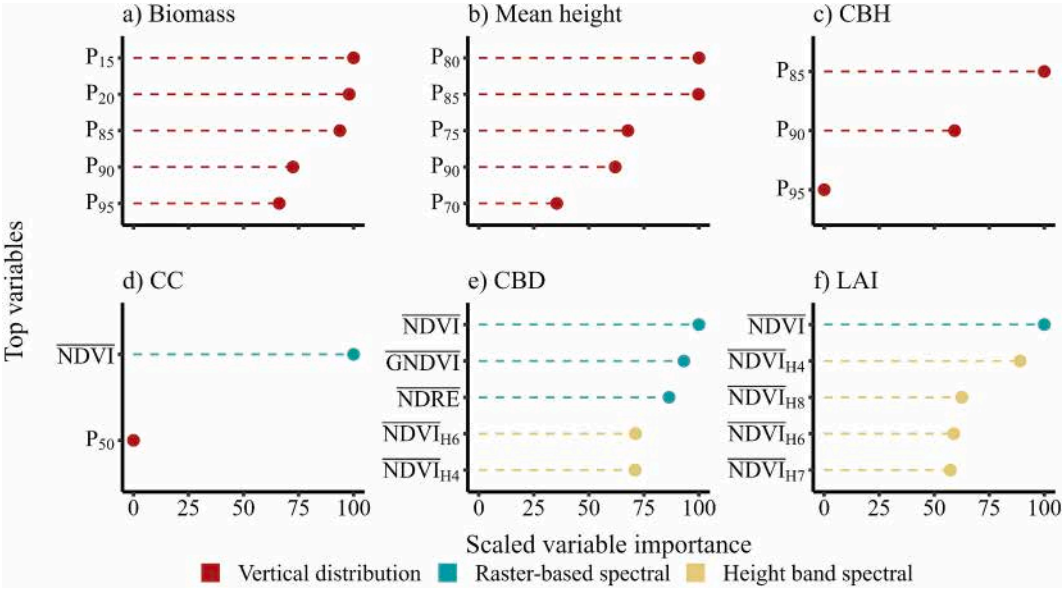

Fig. 8. Relative scaled importance of top five predictors for random forest models produced across all sites.

4. Discussion

Reducing future forest fire hazard and restoring historical fire regimes relies upon the accessibility of accurate spatial information about aboveground biomass and fire fuel loads. Such data are difficult and time consuming to obtain using traditional field-based methods. Instead, the spatial complexity of these environmental attributes lends themselves well to remote sensing approaches. The use of UAS-SfM has the potential to provide a low-cost and flexible means of estimating fuels at stand scales. In a multisite analysis representing a broad range of forest types of California, this study found canopy fuel parameters segregate into two distinct groups, as identified by field measurement correlations, and this separation consistently emerged in model analyses. Specifically, model performances and variable selection displayed

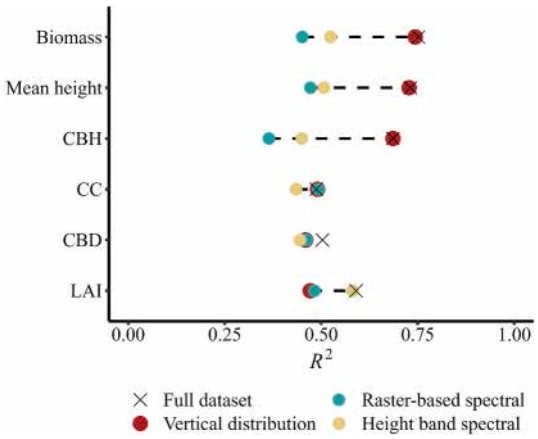

Fig. 9. Random forest all-sites model accuracy produced using different predictor variable subsets, including the full-predictor dataset. Performance results obtained from 100 replicates of 10-fold cross validation using spatially-blocked groups.

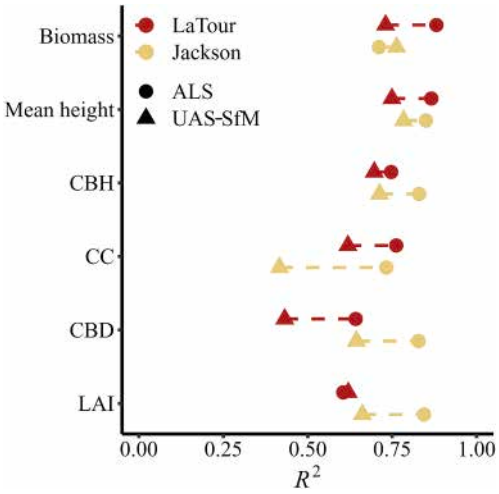

Fig. 10. UAS-SfM vs ALS model performance. Random forest individual site model results from 100 replicates of 5-fold cross validation without spatial blocking.

Table 4
Model accuracy when applied to a novel site withheld from training. Model generated using 100 replicates of 10-fold cross validation using spatially-blocked groups from all sites except Saddle Mountain. Saddle Mountain accuracy metrics derived from the application of this model to the site without further training.

Canopy fuel parameter	R^2		RMSE	
	Model	Saddle Mtn	Model	Saddle Mtn
Biomass	0.82	0.74	8.89	14.71
Mean height	0.79	0.84	4.25	6.31
CBH	0.74	0.69	2.60	2.40
CC	0.65	0.05	11.01	8.20
CBD	0.55	0.20	0.020	0.010
LAI	0.60	0.31	1.18	1.15

close similarity within groups but differed markedly between them. All modelling methods exhibited this same performance disparity between groups. Random forest and SVM selected the same sets of distinct predictors for the two groups, but linear regression methods did not display a pattern in variable selection. The first group is comprised of the vertical structure parameters biomass, mean height, and CBH. The second group contains the horizontal structure parameters canopy cover, CBD, and LAI.

In models built using the combined data from all study sites, random forest consistently returned the highest overall accuracy, as defined by R^2 and RMSE, compared to SVM or linear regression methods. This is consistent with previous research identifying the performance of this method in similar applications (e.g., de Almeida et al., 2019; Arellano-Pérez et al., 2018). Since random forest is unable to extrapolate beyond the range of the data used to train the model, cross-validation error increased substantially for extreme parameter values. This limitation also restricted our novel site testing to the only site (Saddle Mountain) whose parameters fell within the range bounded by the other three sites. This challenge is not specific to random forest and highlights the importance of sampling breadth and distribution when targeting an area of interest or when applying a model to novel areas.

4.1. *Vertical structure: biomass, CBH, mean height*

Our model for CBH exceeded previously published photogrammetric model accuracies by >20% (Filippelli et al., 2019; Shin et al., 2018), and our models for biomass and mean canopy height fell within 2% of the highest previously published performance metrics for UAS-SfM or photogrammetry derived models from forest ecosystems around the world (Domingo et al., 2019; Filippelli et al., 2019; Ota et al., 2019; Shin et al., 2018), including previous work in California forests (Lamping et al., 2021).

The performance of the model for CBH demonstrates the powerful utility of combining machine learning with UAS-SfM to overcome SfM's inherent limited capacity to measure subcanopy forest structure (Forbes et al., 2022; Reilly et al., 2021) by exploiting inherent relationships in the canopy to model attributes that otherwise elude direct detection by photogrammetric methods (Filippelli et al., 2019). Shin et al. (2018) only achieved 33% accuracy in their attempt to model CBH using a single lower canopy height predictor derived from UAS-SfM data. In our study, however, the random forest model for CBH leveraged the observed relationship in the field data between CBH and mean height to achieve a high accuracy for a key canopy fuel parameter that it otherwise was unable to directly observe. Future research should investigate whether this indirect approach can detect the effects of targeted understory treatments, such as thinning or prescribed burns.

The UAS-SfM models for these three vertical fuel parameters demonstrated comparable accuracy to those using ALS predictors at the two sites included in this analysis. Our UAS-SfM models for CBH and mean height only marginally underperformed ALS models at the test sites of Jackson and LaTour, and fell within the range of globally reported ALS model accuracies for these parameters (Alonso-Rego et al., 2021; Andersen et al., 2005; Botequim et al., 2019; Bright et al., 2017; Chamberlain et al., 2021; Engelstad et al., 2019; Erdody and Moskal, 2010). Of note, the UAS-SfM model for biomass at Jackson outperformed its ALS counterpart and our full-predictor UAS-SfM biomass model outperformed previously published ALS-based models from California forest sites and from other Mediterranean-climate regions (Alonso-Rego et al., 2021; Lamping et al., 2021). This finding aligns with previous results demonstrating that UAS-SfM and photogrammetry based models of biomass match or outperform ALS models in ponderosa pine forests in the western United States (Filippelli et al., 2019; Swayze et al., 2022). Since biomass is partially determined by canopy height, the higher point density of UAS-SfM (e.g., 320 points/m^2) at the top of canopy may render it particularly well suited for measuring total tree height, whereas lower ALS point density (e.g., 25 points/m^2) could result in missing maximum measurements of treetops. For this set of vertical canopy fuel parameters, these results suggest UAS-SfM area-based random forest models can provide comparable accuracy to ALS based methods and may outperform ALS under certain conditions.

Reflecting the vertical structural nature of these parameters, the top variables selected by the model for each parameter consisted solely of

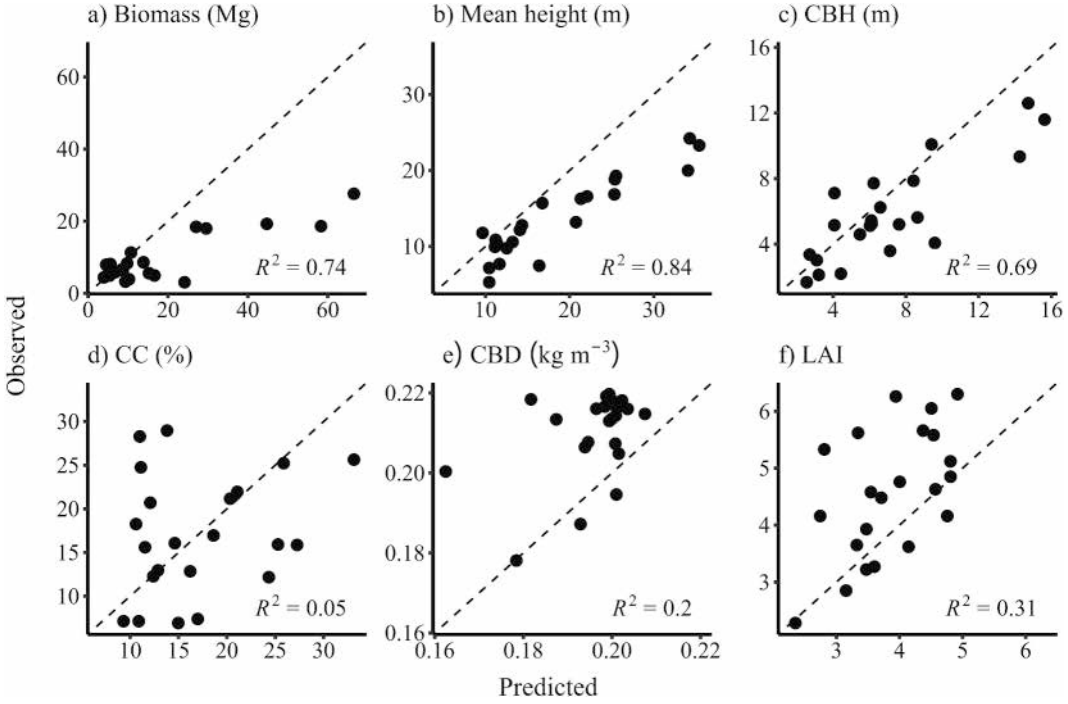

Fig. 11. Saddle Mountain random forest model transfer accuracy. Dotted reference line denotes idealized one-to-one relationship between measured and predicted values.

point cloud height percentiles and model performances were negligibly affected by the removal of spectral data in the predictor subset analysis. Other studies have reported similar structural variable selection for these parameters (e.g., Lamping et al., 2021; Swayze et al., 2022). Additionally, when applied to a novel site, these models retained a high level of performance. This suggests the vertical distribution predictor relationships identified by the random forest models persist across sites and among forest types. Consequently, these vertical structure canopy fuel parameters are well suited to 3D-based mapping approaches and the addition of spectral information does not significantly affect model accuracy.

4.2. *Horizontal structure: LAI, CBD, canopy cover*

The horizontal structure parameters of LAI, CBD, and canopy cover demonstrated consistently lower model accuracy than the vertical structure parameters, never exceeding R^2 of 0.60 for any of the random forest models. In contrast to the vertical parameters, the random forest models for these horizontal parameters relied upon spectral attributes of the UAS-SfM data, with raster-based mean NDVI arising as the top contributor in all models. These horizontal parameters pertain directly to aspects of the forest canopy, namely its composition, spatial distribution, and density of live and dead leaves and branches. Consequently, it appears that these random forest models leveraged the relationships between spectral indices and live-canopy characteristics, such as concentration of photosynthetic activity, to model these plot-scale horizontal attributes.

Our canopy cover model accuracy falls below the lowest previously published UAS-SfM derived canopy cover models from forests around the globe (Belmonte et al., 2019; Shin et al., 2018; Wallace et al., 2019; Zahra et al., 2022). However, Belmonte et al. (2019) demonstrated a significant 30% decrease in model performance with increasing canopy cover in ponderosa pine forests, with accuracy dropping to match our results in their highest density stands. Considering that only the Pepperwood site contained a majority of plots below their high-density threshold, our results align with the Belmonte et al. finding that UAS-SfM struggles to model canopy cover under high-cover conditions. For this parameter, plot level mean NDVI appears to represent a proxy for percentage of live canopy in relation to ground and below-canopy senesced vegetation or exposed soil. This finding aligns with other studies that have identified NDVI as a highly accurate single predictor for canopy cover from UAS-SfM (Shin et al., 2018; Zahra et al., 2022). ALS, on the other hand, is particularly well suited for mapping canopy cover since it is able to actively detect subcanopy structure regardless of level of cover and, globally, has reported accuracies >99% (Cai et al., 2021; Dai et al., 2022).

For CBD, our modelling approach utilizing spectral indices returned a significant improvement over previous literature. Few existing studies have modelled CBD using photogrammetric techniques and, to our knowledge, only Shin et al. (2018) utilized UAS-SfM for this purpose. Shin et al. (2018) only achieved an accuracy of <1% in ponderosa pine forest in their attempt to reconstruct CBD through allometric equations based on their UAS-SfM derived measurements of canopy height. Consequently, this study's demonstrated accuracy of 50% represents a significant improvement in performance over this previous UAS-SfM study and also exceeds the highest photogrammetric accuracy in the literature (Filippelli et al., 2019). Our demonstrated increase in performance over these previous studies likely arises from the utilization of predictors derived from the multispectral data and spectral indices included in this study that were absent from these previous works. The power of these predictors, in turn, was further augmented by the machine learning methods we employed, specifically random forest, as compared to the allometric reconstruction approach used by Shin et al. (2018) or the linear regression method (without stepwise predictor selection) utilized by Filippelli et al. (2019). In accordance with our observed lower UAS-SfM performance compared to our ALS models of CBD, our UAS-SfM model accuracy is at the bottom end of published ALS CBD models from around the world (Alonso-Rego et al., 2021; Andersen et al., 2005; Bright et al., 2017; Chamberlain et al., 2021; Engelstad et al., 2019; García et al., 2017). We further note that CBD is difficult to measure in the field, and CBD model uncertainty is further increased by the weak relationship in the equations from Keane et al. (2005) used to estimate CBD from LAI-2000 gap fraction, and the model's focus on conifer forests.

While our model for LAI performed better than those of the other horizontal parameters, it underperformed compared to previously published photogrammetry models (Li et al., 2022; Liu and Wang, 2018; Stobbelaar et al., 2022; Zhang et al., 2019) and ALS models (e.g., Sumnall et al., 2021; Wang et al., 2023; Yin et al., 2022) from forests around the world. The previous photogrammetric studies were conducted within single forest types. Consequently, our lower performance may be due to the breadth of forest types represented in our multi-site analysis. Further, as with CBD, LAI was estimated based on an equation applied to LAI-2000 gap fraction measurements, and factors such as variable overhead sunlight conditions could add to model error. However, the saturation of spectral indices presents a much more likely mechanism for this decline in model accuracy. In models from forest sites around the globe, satellite-based NDVI has been demonstrated to possess the strongest relationship with LAI field measurements when LAI values are below two, and NDVI becomes asymptotically saturated when LAI rises further (Gao et al., 2023; Haboudane, 2004). Only Pepperwood had a majority of plots with LAI below this level. As a result, our model of LAI displayed a sharp prediction threshold as LAI increased above three, strongly suggesting the impact of this oversaturation effect influenced the performance of our models.

Models for all three canopy fuel parameters followed a similar trend in performance, exhibiting a clustering of model predictions and loss of accuracy at the highest end of their respective ranges, suggesting this impact of oversaturation to be ubiquitous. In the novel site testing at Saddle Mountain, model performance declined considerably for all three parameters. The Saddle Mountain plots fall at the top end of the observed range for this group. Since random forest cannot extrapolate, this error at the end of the range could be an artifact of insufficient training data at elevated fuel parameter levels such as high canopy cover. Additionally, since our novel site testing was limited to a single site, this decline in model performance could also be due to some undetected irregularity of the plots at Saddle Mountain. However, the most likely explanation for this failure is the aforementioned loss of information due to the oversaturation of spectral indices.

In the predictor subset analysis for the horizontal fuels, both the spectral-based vertical distribution and raster-based models returned comparable accuracy to one another for all three parameters. The raster-based model variable selection resembled the top variables from the full predictor models and, once again, all models identified mean NDVI as the key predictor. The model with vertical distribution predictors selected top variables relating to the point distribution within the middle third of the canopy, pointing to the relationship between the bulk distribution of the point cloud and these horizontal canopy fuel parameters. However, despite their performance in subset models, the combination of the spectral and vertical data in the full-predictor model did not significantly improve the accuracy beyond that of the subset models for canopy cover or CBD. LAI was the only fuel parameter for which the combined structural and spectral capacity of UAS-SfM appeared to significantly impact overall model performance. Based on these findings, future studies into horizontal canopy fuel parameters should prioritize the multispectral capabilities of UAS-SfM.

4.3. Future research

As stated previously, the random forest models for vertical fuel parameters relied exclusively upon point cloud height percentile predictors, with no improvement from the addition of spectral data. Future photogrammetric studies into this parameter set, therefore, should focus on sensors that prioritize image resolution and view angle (e.g., high-definition RGB cameras with view angle control), rather than spectral breadth, to maximize canopy structure detection. Furthermore, this sensor selection could provide higher sub-canopy structure detection, and therefore potentially greater model accuracy, through the collection of oblique imagery beyond the capabilities of the nadir restricted Micasense RedEdge-MX sensor employed in this study (Wallace et al., 2019). Other lidar methods, such as UAS or terrestrial lidar, could also be explored to determine the range of achievable accuracies with this area-based multisite modelling approach.

In contrast, since the models for LAI, CBD, and canopy cover solely utilized spectral indices, modelling using satellite-based spectral data may be able to provide comparable accuracies to those observed in this study. The 0.04 ha scale of the ground validation plots underlying this study dictated the spatial resolution at which the UAS-SfM modelling could be performed. Consequently, despite its high-resolution, reducing the UAS-SfM data to a matching spatial resolution could have resulted in potentially significant loss of detail and accuracy, potentially exacerbating an already weak information signal due to the oversaturation of spectral indices. The 0.04 ha resolution at which these analyses were conducted is comparable to that provided by modern satellite multispectral sensors, such as Landsat 8–9 and Sentinel 2. (e.g., Drusch et al., 2012). In post-fire mapping applications, Sentinel-2 derived NDVI has been demonstrated to correspond to coincidental measurements obtained from multispectral UAS-SfM (Pádua et al., 2020). Consequently, models built using these satellite-based spectral indices could match the performance accuracy to the methods employed in this study (Arellano-Pérez et al., 2018; Chuvieco et al., 2020; Gale et al., 2021), with the advantage of greater temporal frequency and spatial extent for lower monetary cost. For example, while they failed to model vertical canopy fuels, Pierce et al. (2012) successfully modelled CBD and canopy cover at a site neighboring LaTour using Landsat derived indices. The additional spectral bands, and therefore potential indices, available via satellite sensors could assist in mitigating the oversaturation that may have hampered our models (Gao et al., 2023). Future studies should further investigate the capacity of these direct modelling approaches using satellite spectral indices for horizontal canopy fuels since the accessibility of these data would render them of high value to land managers, particularly in tracking change over larger areas or with greater frequency than is feasible with UAS-SfM. However, the decreased accuracy of our spectra-based models when applied to a novel site testing scenario suggests that the spatial and temporal consistency of these methods requires extensive validation prior to being employed for operational applications.

Lastly, future studies could also explore the potential of deeper machine learning approaches such as convoluted neural networks (CNN) to model fuel parameters (e.g., Talebiesfandarani and Shamsoddini, 2022; Tian et al., 2024; Zhang et al., 2022). Our random forest model for CBD outperformed previous models in the literature, in part due to our utilization of a more complex modelling approach, and measures of variable importance and partial dependency in this technique provide model interpretability. Consequently, it may be possible for more advanced modelling approaches to provide even greater performance than observed here, although the feature and decision space in these approaches may be less interpretable (e.g., SVM, CNN). However, the sample size required to train these models presents a prohibitive barrier to their implementation.

4.4. Conclusions

This study presents novel analysis of UAS-SfM structural and multispectral area-based machine learning models of biomass and canopy fuel parameters across a broad range of complex forest types characteristic of California and other Mediterranean regions. We found the following:

- Fuel parameters segregate into vertical (biomass, CBH, and mean height) and horizontal (LAI, CBD, canopy cover) groups based on correlations between field measurements and these relationships persist throughout model results.
- UAS-SfM random forest models are well suited for modelling the vertical structure canopy fuels parameters. These models retained high performance in comparison to ALS and when transferred to a novel site.

- Models for vertical fuel parameters rely exclusively upon UAS-SfM vertical structure predictors and exhibit no model improvement with the addition of spectral predictors. Future studies on this group, therefore, should focus on image resolution to improve structural information gathering, rather than spectral resolution.
- UAS-SfM random forest models provided less accurate estimates of the horizontal structure parameters. In addition, these models exhibited significant loss in accuracy in comparison to ALS and in the novel site transfer.
- Models for horizontal fuel parameters rely primarily upon raster-based spectral indices, primarily NDVI. Due to the similarity between the plot size in this study and satellite imagery resolution, future work should explore if models using satellite-based spectral data can provide comparable performance to the UAS-SfM spectral results presented here.

The mitigation of wildfire hazard and restoration of historical fire regimes in the forests of California, USA relies upon the accessibility of accurate data on the spatial distribution of fuel loads to inform management decision making. Canopy fuel parameters present a critical component of forest structure for these purposes since they moderate crown torching and sustained ignition, hallmarks of high severity fire events. Future work should expand on these results to ascertain better methods for performing widespread mapping coverage and developing models that are robust to transfer to novel sites. These two factors will significantly improve the operational use of these methods by land managers. In our case, our ability to generate widespread maps was limited to Pepperwood due to the landing requirements of the fixed-wing drone and the battery limitations of the quadcopter. However, future research using new UAS technology such as vertical takeoff and landing fixed-wing drones will be able to overcome these limitations and generate meaningfully large maps for ongoing management monitoring and decision making around fire hazard mitigation.

CRediT authorship contribution statement

Sean Reilly: Writing – original draft, Visualization, Software, Methodology, Investigation, Formal analysis, Conceptualization. **Matthew L. Clark:** Writing – review & editing, Supervision, Software, Resources, Methodology, Investigation, Funding acquisition, Formal analysis, Conceptualization. **Lika Loechler:** Writing – review & editing, Investigation. **Jack Spillane:** Writing – review & editing, Investigation. **Melina Kozanitas:** Writing – review & editing, Investigation. **Paris Krause:** Writing – review & editing, Investigation. **David Ackerly:** Writing – review & editing, Resources. **Lisa Patrick Bentley:** Writing – review & editing, Resources, Funding acquisition. **Imma Oliveras Menor:** Writing – review & editing, Supervision, Methodology.

Declaration of competing interest

The authors declare that they have no known competing financial interests or personal relationships that could have appeared to influence the work reported in this paper.

Data availability

UAS-SfM data are available at Zenodo https://doi.org/10.5281/zenodo.12809155. Field data and analysis R code can be found on GitHub at https://github.com/seanreilly66/uas_canopy_fuels.

Acknowledgements

Funding for this research was supported by CAL FIRE Forest Health and Forest Legacy (8GG18806) and California State University, Agricultural Research Institute (20-01-106) awards to L.P.B and M.L.C. S.R. was funded by the Rhodes Trust and through the University of Oxford Environmental Change Institute Small Grant Scheme. Pepperwood ground data collection was supported by funding from the Gordon and Betty Moore Foundation and National Science Foundation grants 1754475 and 1835086. We thank Lisa Micheli (Pepperwood Preserve), Monica Delmartini (Saddle Mountain), Jason Poburko (LaTour), and Lynn Webb (Jackson) for granting us use of their sites and facilitating access to their datasets. We thank Ryan Ferrell, Michael O'Neil, Allison Kelly, Brieanne Forbes, Catherine Seel, Corbin Matley in collecting field data and Corbin Matley, Michelle Villasenor, and Natalie Hoover for their assistance in collecting UAS data. We also thank Andrew Peters for his work on the study site map.

Appendix A. Supplementary data

Supplementary data to this article can be found online at https://doi.org/10.1016/j.rse.2024.114310.

References

Aasen, H., Honkavaara, E., Lucieer, A., Zarco-Tejada, P.J., 2018. Quantitative remote sensing at ultra-high resolution with UAV spectroscopy: a review of sensor technology, measurement procedures, and data correction workflows. Remote Sens. 10, 1091. https://doi.org/10.3390/rs10071091.

Abdollahnejad, A., Panagiotidis, D., 2020. Tree species classification and health status assessment for a mixed broadleaf-conifer forest with UAS multispectral imaging. Remote Sens. 12, 3722. https://doi.org/10.3390/rs12223722.

Ackerly, D., Oldfather, M., Halbur, M., Micheli, L., 2013. Establishment of Woodland Vegetation Research Plots at Pepperwood Preserve (Technical Report for the Gordon and Betty Moore Foundation). Dwight Center for Conservation Science, Pepperwood, Santa Rosa, CA.

Ackerly, D.D., Kling, M.M., Clark, M.L., Papper, P., Oldfather, M.F., Flint, A.L., Flint, L.E., 2020. Topoclimates, refugia, and biotic responses to climate change. Front. Ecol. Environ. 18, 288–297. https://doi.org/10.1002/fee.2204.

Adjidjonu, D., Burgett, J., 2021. Assessing the accuracy of unmanned aerial vehicles photogrammetric survey. Int. J. Constr. Educ. Res. 17, 85–96. https://doi.org/10.1080/15578771.2020.1717683.

Agee, J.K., Skinner, C.N., 2005. Basic principles of forest fuel reduction treatments. For. Ecol. Manag. 211, 83–96. https://doi.org/10.1016/j.foreco.2005.01.034.

Agüera-Vega, F., Carvajal-Ramírez, F., Martínez-Carricondo, P., 2017. Accuracy of digital surface models and orthophotos derived from unmanned aerial vehicle photogrammetry. J. Surv. Eng. 143, 04016025. https://doi.org/10.1061/(ASCE)SU.1943-5428.0000206.

Alonso-Rego, C., Arellano-Pérez, S., Guerra-Hernández, J., Molina-Valero, J.A., Martínez-Calvo, A., Pérez-Cruzado, C., Castedo-Dorado, F., González-Ferreiro, E., Álvarez-González, J.G., Ruiz-González, A.D., 2021. Estimating stand and fire-related surface and canopy fuel variables in pine stands using low-density airborne and single-scan terrestrial laser scanning data. Remote Sens. 13, 5170. https://doi.org/10.3390/rs13245170.

Alonzo, M., Andersen, H.-E., Morton, D., Cook, B., 2018. Quantifying boreal forest structure and composition using UAV structure from motion. Forests 9, 119. https://doi.org/10.3390/f9030119.

Andersen, H.-E., McGaughey, R.J., Reutebuch, S.E., 2005. Estimating forest canopy fuel parameters using LIDAR data. Remote Sens. Environ. 94, 441–449. https://doi.org/10.1016/j.rse.2004.10.013.

Aragoneses, E., Chuvieco, E., 2021. Generation and mapping of fuel types for fire risk assessment. Fire 4, 59. https://doi.org/10.3390/fire4030059.

Arellano-Pérez, S., Castedo-Dorado, F., López-Sánchez, C., González-Ferreiro, E., Yang, Z., Díaz-Varela, R., Álvarez-González, J., Vega, J., Ruiz-González, A., 2018. Potential of sentinel-2A data to model surface and canopy fuel characteristics in relation to crown fire hazard. Remote Sens. 10, 1645. https://doi.org/10.3390/rs10101645.

Arroyo, L.A., Pascual, C., Manzanera, J.A., 2008. Fire models and methods to map fuel types: the role of remote sensing. For. Ecol. Manag. 256, 1239–1252. https://doi.org/10.1016/j.foreco.2008.06.048.

Beaty, R.M., Taylor, A.H., 2008. Fire history and the structure and dynamics of a mixed conifer forest landscape in the northern Sierra Nevada, Lake Tahoe Basin, California, USA. For. Ecol. Manag. 255, 707–719. https://doi.org/10.1016/j.foreco.2007.09.044.

Belmonte, A., Sankey, T., Biederman, J.A., Bradford, J., Goetz, S.J., Kolb, T., Woolley, T., 2019. UAV-derived estimates of forest structure to inform ponderosa pine forest restoration. Remote Sens. Ecol. Conservat. https://doi.org/10.1002/rse2.137.

Berbach, M., Cafferata, P., Schlosser, J., Eng, H., Robards, T., McDonald, S., Walters, D., Dreesmann, K., 1995. Latour Demonstration State Forest Sustained Yield Plan. California Department of Forestry and Fire Protection.

Botequim, B., Fernandes, P.M., Borges, J.G., González-Ferreiro, E., Guerra-Hernández, J., 2019. Improving silvicultural practices for Mediterranean forests through fire behaviour modelling using LiDAR-derived canopy fuel characteristics. Int. J. Wildland Fire 28, 823. https://doi.org/10.1071/WF19001.

Breiman, L., 2001. Random forests. Mach. Learn. 45, 5–32. https://doi.org/10.1023/A:1010933404324.

Bright, B., Hudak, A., Meddens, A., Hawbaker, T., Briggs, J., Kennedy, R., 2017. Prediction of forest canopy and surface fuels from lidar and satellite time series data in a bark beetle-affected forest. Forests 8, 322. https://doi.org/10.3390/f8090322.
Cai, S., Zhang, W., Jin, S., Shao, J., Li, L., Yu, S., Yan, G., 2021. Improving the estimation of canopy cover from UAV-LiDAR data using a pit-free CHM-based method. Int. J. Digit. Earth 14, 1477–1492. https://doi.org/10.1080/17538947.2021.1921862.
Chamberlain, C.P., Sánchez Meador, A.J., Thode, A.E., 2021. Airborne lidar provides reliable estimates of canopy base height and canopy bulk density in southwestern ponderosa pine forests. For. Ecol. Manag. 481, 118695 https://doi.org/10.1016/j.foreco.2020.118695.
Chandrasekaran, A., Shao, G., Fei, S., Miller, Z., Hupy, J., 2022. Automated inventory of broadleaf tree plantations with UAS imagery. Remote Sens. 14, 1931. https://doi.org/10.3390/rs14081931.
Chávez-Durán, Á.A., García, M., Olvera-Vargas, M., Aguado, I., Figueroa-Rangel, B.L., Trucíos-Caciano, R., Rubio-Camacho, E.A., 2024. Forest canopy fuel loads mapping using unmanned aerial vehicle high-resolution red, green, blue and multispectral imagery. Forests 15, 225. https://doi.org/10.3390/f15020225.
Chuvieco, E., Aguado, I., Salas, J., García, M., Yebra, M., Oliva, P., 2020. Satellite remote sensing contributions to wildland fire science and management. Curr. Forestr. Rep. 6, 81–96. https://doi.org/10.1007/s40725-020-00116-5.
Collins, B.M., Miller, J.D., Thode, A.E., Kelly, M., van Wagtendonk, J.W., Stephens, S.L., 2009. Interactions among wildland fires in a long-established Sierra Nevada natural fire area. Ecosystems 12, 114–128. https://doi.org/10.1007/s10021-008-9211-7.
Collins, B.M., Stephens, S.L., Moghaddas, J.J., Battles, J., 2010. Challenges and approaches in planning fuel treatments across fire-excluded forested landscapes. J. For. 108, 24–31. https://doi.org/10.1093/jof/108.1.24.
Cressie, N., 1988. Spatial prediction and ordinary kriging. Math. Geol. 20.
Cutler, F., Original by L.B. and A., Wiener, R. Port by A.L. and M, 2022. Randomforest: Breiman and Cutler's Random Forests for Classification and Regression.
Dai, W., Guan, Q., Cai, S., Liu, R., Chen, R., Liu, Q., Chen, C., Dong, Z., 2022. A comparison of the performances of unmanned-aerial-vehicle (UAV) and terrestrial laser scanning for forest plot canopy cover estimation in Pinus massoniana forests. Remote Sens. 14, 1188. https://doi.org/10.3390/rs14051188.
Dash, J.P., Pearse, G.D., Watt, M.S., 2018. UAV multispectral imagery can complement satellite data for monitoring forest health. Remote Sens. 10, 1216. https://doi.org/10.3390/rs10081216.
de Almeida, C.T., Galvão, L.S., Aragão, L.E.D.E., Ometto, J.P.H.B., Jacon, A.D., Pereira, F. R.D., Sato, L.Y., Lopes, A.P., Graça, P.M.L.D., Silva, C.V.D., Ferreira-Ferreira, J., Longo, M., 2019. Combining LiDAR and hyperspectral data for aboveground biomass modeling in the Brazilian Amazon using different regression algorithms. Remote Sens. Environ. 232, 111323 https://doi.org/10.1016/j.rse.2019.111323.
Dennison, P.E., Brewer, S.C., Arnold, J.D., Moritz, M.A., 2014. Large wildfire trends in the western United States, 1984-2011. Geophys. Res. Lett. 41, 2928–2933. https://doi.org/10.1002/2014GL059576.
Dewberry, 2018. California FEMA F9 Lidar Report (No. G17PD00044).
Domingo, Ørka, Næsset, Kachamba, Gobakken, 2019. Effects of UAV image resolution, camera type, and image overlap on accuracy of biomass predictions in a tropical woodland. Remote Sens. 11, 948. https://doi.org/10.3390/rs11080948.
Drusch, M., Del Bello, U., Carlier, S., Colin, O., Fernandez, V., Gascon, F., Hoersch, B., Isola, C., Laberinti, P., Martimort, P., Meygret, A., Spoto, F., Sy, O., Marchese, F., Bargellini, P., 2012. Sentinel-2: ESA's optical high-resolution mission for GMES operational services. Remote Sens. Environ. 120, 25–36. https://doi.org/10.1016/j.rse.2011.11.026.
Duff, T., Keane, R., Penman, T., Tolhurst, K., 2017. Revisiting wildland fire fuel quantification methods: the challenge of understanding a dynamic, biotic entity. Forests 8, 351. https://doi.org/10.3390/f8090351.
Eng, H., 2015. Jackson Demonstration State Forest, California, United States of America. In: Forest Plans of North America. Elsevier, pp. 177–187. https://doi.org/10.1016/B978-0-12-799936-4.00021-7.
Engelstad, P.S., Falkowski, M., Wolter, P., Poznanovic, A., Johnson, P., 2019. Estimating canopy fuel attributes from low-density LiDAR. Fire 2, 38. https://doi.org/10.3390/fire2030038.
Erdody, T.L., Moskal, L.M., 2010. Fusion of LiDAR and imagery for estimating forest canopy fuels. Remote Sens. Environ. 114, 725–737. https://doi.org/10.1016/j.rse.2009.11.002.
Evett, R.R., Dawson, A., Bartolome, J.W., 2013. Estimating vegetation reference conditions by combining historical source analysis and soil phytolith analysis at pepperwood preserve, northern California coast ranges, U.S.A: estimating vegetation reference conditions. Restor. Ecol. 21, 464–473. https://doi.org/10.1111/j.1526-100X.2012.00912.x.
FIA, 2014. Regional Biomass Equations Used by FIA to Estimate Bole, Bark, and Branches. U.S. Department of Agriculture Forest Service, Pacific Northwest Research Station.
Filippelli, S.K., Lefsky, M.A., Rocca, M.E., 2019. Comparison and integration of lidar and photogrammetric point clouds for mapping pre-fire forest structure. Remote Sens. Environ. 224, 154–166. https://doi.org/10.1016/j.rse.2019.01.029.
Forbes, B., Reilly, S., Clark, M., Ferrell, R., Kelly, A., Krause, P., Matley, C., O'Neil, M., Villasenor, M., Disney, M., Wilkes, P., Bentley, L.P., 2022. Comparing remote sensing and field-based approaches to estimate ladder fuels and predict wildfire burn severity. Front. For. Glob. Chang. 5, 818713 https://doi.org/10.3389/ffgc.2022.818713.
Foster, D.E., Battles, J.J., Collins, B.M., York, R.A., Stephens, S.L., 2020. Potential wildfire and carbon stability in frequent-fire forests in the Sierra Nevada: trade-offs from a long-term study. Ecosphere 11. https://doi.org/10.1002/ecs2.3198.
Fraser, B.T., Congalton, R.G., 2018. Issues in unmanned aerial systems (UAS) data collection of complex forest environments. Remote Sens. 10, 908. https://doi.org/10.3390/rs10060908.
Fu, X., Zhang, Z., Cao, L., Coops, N.C., Goodbody, T.R.H., Liu, H., Shen, X., Wu, X., 2021. Assessment of approaches for monitoring forest structure dynamics using bi-temporal digital aerial photogrammetry point clouds. Remote Sens. Environ. 255, 112300 https://doi.org/10.1016/j.rse.2021.112300.
Gale, M.G., Cary, G.J., Van Dijk, A.I.J.M., Yebra, M., 2021. Forest fire fuel through the lens of remote sensing: review of approaches, challenges and future directions in the remote sensing of biotic determinants of fire behaviour. Remote Sens. Environ. 255, 112282 https://doi.org/10.1016/j.rse.2020.112282.
Gao, Si, Zhong, R., Yan, K., Ma, X., Chen, X., Pu, J., Gao, Sicong, Qi, J., Yin, G., Myneni, R.B., 2023. Evaluating the saturation effect of vegetation indices in forests using 3D radiative transfer simulations and satellite observations. Remote Sens. Environ. 295, 113665 https://doi.org/10.1016/j.rse.2023.113665.
García, M., Saatchi, S., Casas, A., Koltunov, A., Ustin, S., Ramirez, C., Balzter, H., 2017. Extrapolating forest canopy fuel properties in the California rim fire by combining airborne lidar and Landsat OLI data. Remote Sens. 9, 394. https://doi.org/10.3390/rs9040394.
García-Cimarras, A., Manzanera, J.A., Valbuena, R., 2021. Analysis of Mediterranean vegetation fuel type changes using multitemporal LiDAR. Forests 12, 335. https://doi.org/10.3390/f12030335.
Griffith, G.E., Omernik, J.M., Smith, D.W., Cook, T.D., Tallyn, E., Moseley, K., Johnson, C.B., 2016. Ecoregions of California (Report No. 2016–1021), Open-File Report. Reston, VA. https://doi.org/10.3133/ofr20161021.
Haboudane, D., 2004. Hyperspectral vegetation indices and novel algorithms for predicting green LAI of crop canopies: modeling and validation in the context of precision agriculture. Remote Sens. Environ. 90, 337–352. https://doi.org/10.1016/j.rse.2003.12.013.
Hessburg, P.F., Churchill, D.J., Larson, A.J., Haugo, R.D., Miller, C., Spies, T.A., North, M.P., Povak, N.A., Belote, R.T., Singleton, P.H., Gaines, W.L., Keane, R.E., Aplet, G.H., Stephens, S.L., Morgan, P., Bisson, P.A., Rieman, B.E., Salter, R.B., Reeves, G.H., 2015. Restoring fire-prone inland Pacific landscapes: seven core principles. Landsc. Ecol. 30, 1805–1835. https://doi.org/10.1007/s10980-015-0218-0.
Hillman, S., Wallace, L., Lucieer, A., Reinke, K., Turner, D., Jones, S., 2021a. A comparison of terrestrial and UAS sensors for measuring fuel hazard in a dry sclerophyll forest. Int. J. Appl. Earth Obs. Geoinf. 95, 102261 https://doi.org/10.1016/j.jag.2020.102261.
Hillman, S., Wallace, L., Reinke, K., Jones, S., 2021b. A comparison between TLS and UAS LiDAR to represent eucalypt crown fuel characteristics. ISPRS J. Photogramm. Remote Sens. 181, 295–307. https://doi.org/10.1016/j.isprsjprs.2021.09.008.
Hunter, M.E., Robles, M.D., 2020. Tamm review: the effects of prescribed fire on wildfire regimes and impacts: a framework for comparison. For. Ecol. Manag. 475, 118435 https://doi.org/10.1016/j.foreco.2020.118435.
Husari, S., Nichols, H.T., Sugihara, N.G., Stephens, S.L., 2006. Fire and fuel management. In: Sugihara, N. (Ed.), Fire in California's Ecosystems. University of California Press, pp. 444–465. https://doi.org/10.1525/california/9780520246058.003.0019.
Karatzoglou, A., Smola, A., Hornik, K., Australia (NICTA), N.I., Maniscalco, M.A., Teo, C. H, 2023. Kernlab: Kernel-Based Machine Learning Lab.
Keane, R.E., Reinhardt, E.D., Scott, J., Gray, K., Reardon, J., 2005. Estimating forest canopy bulk density using six indirect methods. Can. J. For. Res. 35, 724–739. https://doi.org/10.1139/x04-213.
Keeley, J.E., Fotheringham, C.J., Morais, M., 1999. Reexamining fire suppression impacts on brushland fire regimes. Science 284, 1829–1832. https://doi.org/10.1126/science.284.5421.1829.
Kramer, H., Collins, B., Kelly, M., Stephens, S., 2014. Quantifying ladder fuels: a new approach using LiDAR. Forests 5, 1432–1453. https://doi.org/10.3390/f5061432.
Kuhn, M., Wing, J., Weston, S., Williams, A., Keefer, C., Engelhardt, A., Cooper, T., Mayer, Z., Kenkel, B., R Core Team, Benesty, M., Lescarbeau, R., Ziem, A., Scrucca, L., Tang, Y., Candan, C., Hunt, T., 2023. Caret: Classification and Regression Training.
Lamping, J.E., Zald, H.S.J., Madurapperuma, B.D., Graham, J., 2021. Comparison of low-cost commercial unpiloted digital aerial photogrammetry to airborne laser scanning across multiple forest types in California, USA. Remote Sens. 13, 4292. https://doi.org/10.3390/rs13214292.
Li, C., Zheng, Y., Zhang, X., Wu, F., Li, L., Jiang, J., 2022. Comparison of canopy cover and leaf area index estimation from airborne lidar and digital aerial photogrammetry in tropical forests. Appl. Sci. 12, 9882. https://doi.org/10.3390/app12199882.
Liu, X., Wang, L., 2018. Feasibility of using consumer-grade unmanned aerial vehicles to estimate leaf area index in mangrove forest. Remote Sens. Lett. 9, 1040–1049. https://doi.org/10.1080/2150704X.2018.1504339.
Lowe, D.G., 2004. Distinctive image features from scale-invariant keypoints. Int. J. Comput. Vis. 60, 91–110. https://doi.org/10.1023/B:VISI.0000029664.99615.94.
Marino, E., Montes, F., Tomé, J.L., Navarro, J.A., Hernando, C., 2018. Vertical forest structure analysis for wildfire prevention: comparing airborne laser scanning data and stereoscopic hemispherical images. Int. J. Appl. Earth Obs. Geoinf. 73, 438–449. https://doi.org/10.1016/j.jag.2018.07.015.
Miller, T.L., Based on F. Code by A, 2020. Leaps: Regression Subset Selection.
Miller, J.D., Safford, H.D., Crimmins, M., Thode, A.E., 2009. Quantitative evidence for increasing forest fire severity in the Sierra Nevada and southern Cascade Mountains, California and Nevada, USA. Ecosystems 12, 16–32. https://doi.org/10.1007/s10021-008-9201-9.
Miller, J.D., Skinner, C.N., Safford, H.D., Knapp, E.E., Ramirez, C.M., 2012. Trends and causes of severity, size, and number of fires in northwestern California, USA. Ecol. Appl. 22, 184–203. https://doi.org/10.1890/10-2108.1.

Minnich, R.A., 1983. Fire mosaics in southern California and northern Baja California. Science 219, 1287–1294. https://doi.org/10.1126/science.219.4590.1287.
Moghaddas, J.J., Roller, G.B., Long, J.W., Saah, D.S., Moritz, M.A., Stark, D.T., Schmidt, D., Buchholz, T., Freed, T.J., Alvey, E.C., Gunn, J.S., 2018. Fuel Treatment for Forest Resilience and Climate Mitigations: A Critical Review for Coniferous Forests of the Sierra Nevada, Southern Cascade, Coast, Klamath, and Transverse Ranges (No. CCCA4- CNRA-2018– 017). California Natural Resources Agency.
Mountrakis, G., Im, J., Ogole, C., 2011. Support vector machines in remote sensing: a review. ISPRS J. Photogramm. Remote Sens. 66, 247–259. https://doi.org/10.1016/j.isprsjprs.2010.11.001.
Navarro, A., Young, M., Allan, B., Carnell, P., Macreadie, P., Ierodiaconou, D., 2020. The application of unmanned aerial vehicles (UAVs) to estimate above-ground biomass of mangrove ecosystems. Remote Sens. Environ. 242, 111747 https://doi.org/10.1016/j.rse.2020.111747.
Oldfather, M.F., Britton, M.N., Papper, P.D., Koontz, M.J., Halbur, M.M., Dodge, C., Flint, A.L., Flint, L.E., Ackerly, D.D., 2016. Effects of topoclimatic complexity on the composition of woody plant communities. AoB Plants 8, plw049. https://doi.org/10.1093/aobpla/plw049.
Ota, T., Ahmed, O.S., Minn, S.T., Khai, T.C., Mizoue, N., Yoshida, S., 2019. Estimating selective logging impacts on aboveground biomass in tropical forests using digital aerial photography obtained before and after a logging event from an unmanned aerial vehicle. For. Ecol. Manag. 433, 162–169. https://doi.org/10.1016/j.foreco.2018.10.058.
Pádua, L., Guimarães, N., Adão, T., Sousa, A., Peres, E., Sousa, J.J., 2020. Effectiveness of Sentinel-2 in multi-temporal post-fire monitoring when compared with UAV imagery. IJGI 9, 225. https://doi.org/10.3390/ijgi9040225.
Park, I.W., Mann, M.L., Flint, L.E., Flint, A.L., Moritz, M., 2021. Relationships of climate, human activity, and fire history to spatiotemporal variation in annual fire probability across California. PLoS One 16, e0254723. https://doi.org/10.1371/journal.pone.0254723.
Parks, S.A., Holsinger, L.M., Miller, C., Nelson, C.R., 2015. Wildland fire as a self-regulating mechanism: the role of previous burns and weather in limiting fire progression. Ecol. Appl. 25, 1478–1492. https://doi.org/10.1890/14-1430.1.
Parks, S.A., Holsinger, L.M., Panunto, M.H., Jolly, W.M., Dobrowski, S.Z., Dillon, G.K., 2018. High-severity fire: evaluating its key drivers and mapping its probability across western US forests. Environ. Res. Lett. 13, 044037 https://doi.org/10.1088/1748-9326/aab791.
Pierce, A.D., Farris, C.A., Taylor, A.H., 2012. Use of random forests for modeling and mapping forest canopy fuels for fire behavior analysis in Lassen volcanic National Park, California, USA. For. Ecol. Manag. 279, 77–89. https://doi.org/10.1016/j.foreco.2012.05.010.
Ploton, P., Mortier, F., Réjou-Méchain, M., Barbier, N., Picard, N., Rossi, V., Dormann, C., Cornu, G., Viennois, G., Bayol, N., Lyapustin, A., Gourlet-Fleury, S., Pélissier, R., 2020. Spatial validation reveals poor predictive performance of large-scale ecological mapping models. Nat. Commun. 11, 4540. https://doi.org/10.1038/s41467-020-18321-y.
Pohjankukka, J., Pahikkala, T., Nevalainen, P., Heikkonen, J., 2017. Estimating the prediction performance of spatial models via spatial k-fold cross validation. Int. J. Geogr. Inf. Sci. 31, 2001–2019. https://doi.org/10.1080/13658816.2017.1346255.
Prichard, S.J., Hessburg, P.F., Hagmann, R.K., Povak, N.A., Dobrowski, S.Z., Hurteau, M. D., Kane, V.R., Keane, R.E., Kobziar, L.N., Kolden, C.A., North, M., Parks, S.A., Safford, H.D., Stevens, J.T., Yocom, L.L., Churchill, D.J., Gray, R.W., Huffman, D.W., Lake, F.K., Khatri-Chhetri, P., 2021. Adapting western North American forests to climate change and wildfires: 10 common questions. Ecol. Appl. 31 https://doi.org/10.1002/eap.2433.
Quantum Spatial, 2020. Carr Hirz Delta Fires 2019 Lidar Processing Report.
R Core Team, 2023. R: A Language and Environment for Statistical Computing.
Reilly, S., Clark, M.L., Bentley, L.P., Matley, C., Piazza, E., Oliveras Menor, I., 2021. The potential of multispectral imagery and 3D point clouds from unoccupied aerial systems (UAS) for monitoring forest structure and the impacts of wildfire in Mediterranean-climate forests. Remote Sens. 13, 3810. https://doi.org/10.3390/rs13193810.
Rocha, K.D., Silva, C.A., Cosenza, D.N., Mohan, M., Klauberg, C., Schlickmann, M.B., Xia, J., Leite, R.V., de Almeida, D.R.A., Atkins, J.W., Cardil, A., Rowell, E., Parsons, R., Sánchez-López, N., Prichard, S.J., Hudak, A.T., 2023. Crown-level structure and fuel load characterization from airborne and terrestrial laser scanning in a longleaf pine (Pinus palustris mill.) forest ecosystem. Remote Sens. 15, 1002. https://doi.org/10.3390/rs15041002.
Roussel, J.-R., Auty, D., De Boissieu, F., Sánchez Meador, A., Jean-François, B., Demetrios, G., Steinmeier, L., Adaszewski, S., 2023. lidR: Airborne Lidar Data manipulation and Visualization for Forestry Applications.
Shaik, R.U., Laneve, G., Fusilli, L., 2022. An automatic procedure for forest fire fuel mapping using hyperspectral (PRISMA) imagery: a semi-supervised classification approach. Remote Sens. 14, 1264. https://doi.org/10.3390/rs14051264.
Shin, P., Sankey, T., Moore, M., Thode, A., 2018. Evaluating unmanned aerial vehicle images for estimating forest canopy fuels in a ponderosa pine stand. Remote Sens. 10, 1266. https://doi.org/10.3390/rs10081266.
Shugart, H.H., Saatchi, S., Hall, F.G., 2010. Importance of structure and its measurement in quantifying function of forest ecosystems. J. Geophys. Res. 115 https://doi.org/10.1029/2009JG000993, 2009JG000993.
Staver, A.C., Archibald, S., Levin, S.A., 2011. The global extent and determinants of savanna and forest as alternative biome states. Science 334, 230–232. https://doi.org/10.1126/science.1210465.
Stefanidou, A., Gitas, I.Z., Katagis, T., 2022. A national fuel type mapping method improvement using sentinel-2 satellite data. Null 37, 1022–1042. https://doi.org/10.1080/10106049.2020.1756460.
Stephens, S.L., Moghaddas, J.J., 2005. Experimental fuel treatment impacts on forest structure, potential fire behavior, and predicted tree mortality in a California mixed conifer forest. For. Ecol. Manag. 215, 21–36. https://doi.org/10.1016/j.foreco.2005.03.070.
Stephens, S.L., Ruth, L.W., 2005. Federal forest-fire policy in the United States. Ecol. Appl. 15, 532–542. https://doi.org/10.1890/04-0545.
Stobbelaar, P., Neinavaz, E., Nyktas, P., 2022. Prediction of leaf area index using thermal infrared data acquired by UAS over a mixed temperate forest. Int. J. Appl. Earth Obs. Geoinf. 114, 103049 https://doi.org/10.1016/j.jag.2022.103049.
Sumnall, M.J., Trlica, A., Carter, D.R., Cook, R.L., Schulte, M.L., Campoe, O.C., Rubilar, R.A., Wynne, R.H., Thomas, V.A., 2021. Estimating the overstory and understory vertical extents and their leaf area index in intensively managed loblolly pine (Pinus taeda L.) plantations using airborne laser scanning. Remote Sens. Environ. 254, 112250 https://doi.org/10.1016/j.rse.2020.112250.
Sun, Z., Wang, Y., Ding, Z., Liang, R., Xie, Y., Li, R., Li, H., Pan, L., Sun, Y., 2023. Individual tree segmentation and biomass estimation based on UAV digital aerial photograph. J. Mt. Sci. 20, 724–737. https://doi.org/10.1007/s11629-022-7563-7.
Swayze, N.C., Tinkham, W.T., Vogeler, J.C., Hudak, A.T., 2021. Influence of flight parameters on UAS-based monitoring of tree height, diameter, and density. Remote Sens. Environ. 263, 112540 https://doi.org/10.1016/j.rse.2021.112540.
Swayze, N.C., Tinkham, W.T., Creasy, M.B., Vogeler, J.C., Hoffman, C.M., Hudak, A.T., 2022. Influence of UAS flight altitude and speed on aboveground biomass prediction. Remote Sens. 14, 1989. https://doi.org/10.3390/rs14091989.
Szpakowski, D., Jensen, J., 2019. A review of the applications of remote sensing in fire ecology. Remote Sens. 11, 2638. https://doi.org/10.3390/rs11222638.
Talebiesfandarani, S., Shamsoddini, A., 2022. Global-scale biomass estimation based on machine learning and deep learning methods. Remote Sens. Applicat.: Soc. Environ. 28, 100868 https://doi.org/10.1016/j.rsase.2022.100868.
Tian, X., Li, J., Zhang, F., Zhang, H., Jiang, M., 2024. Forest aboveground biomass estimation using multisource remote sensing data and deep learning algorithms: a case study over Hangzhou area in China. Remote Sens. 16, 1074. https://doi.org/10.3390/rs16061074.
Van Wagner, C.E., 1977. Conditions for the start and spread of crown fire. Can. J. For. Res. 7, 23–34. https://doi.org/10.1139/x77-004.
Vapnik, V., 2006. Estimation of Dependences Based on Empirical Data, Information Science and Statistics. Springer New York, New York, NY. https://doi.org/10.1007/0-387-34239-7.
Wadoux, A.M.J.-C., Heuvelink, G.B.M., de Bruin, S., Brus, D.J., 2021. Spatial cross-validation is not the right way to evaluate map accuracy. Ecol. Model. 457, 109692 https://doi.org/10.1016/j.ecolmodel.2021.109692.
Wallace, L., Bellman, C., Hally, B., Hernandez, J., Jones, S., Hillman, S., 2019. Assessing the ability of image based point clouds captured from a UAV to measure the terrain in the presence of canopy cover. Forests 10, 284. https://doi.org/10.3390/f10030284.
Wang, Y., Fang, H., Zhang, Y., Li, S., Pang, Y., Ma, T., Li, Y., 2023. Retrieval and validation of vertical LAI profile derived from airborne and spaceborne LiDAR data at a deciduous needleleaf forest site. GISci. & Remote Sens 60, 2214987. https://doi.org/10.1080/15481603.2023.2214987.
Watershed Sciences, 2016. Sonoma County Vegetation Mapping and Lidar Program: Technical Data Report.
Welles, J.M., Norman, J.M., 1991. Instrument for indirect measurement of canopy architecture. Agron. J. 83, 818–825. https://doi.org/10.2134/agronj1991.00021962008300050009x.
Westoby, M.J., Brasington, J., Glasser, N.F., Hambrey, M.J., Reynolds, J.M., 2012. 'Structure-from-motion' photogrammetry: a low-cost, effective tool for geoscience applications. Geomorphology 179, 300–314. https://doi.org/10.1016/j.geomorph.2012.08.021.
Yin, T., Cook, B.D., Morton, D.C., 2022. Three-dimensional estimation of deciduous forest canopy structure and leaf area using multi-directional, leaf-on and leaf-off airborne lidar data. Agric. For. Meteorol. 314, 108781 https://doi.org/10.1016/j.agrformet.2021.108781.
Zahra, N.F., Setiawan, Y., Prasetyo, L.B., 2022. Estimation of mangrove canopy cover using unmanned aerial vehicle (UAV) in Indramayu regency, West Java. IOP Conf. Ser.: Earth Environ. Sci. 950, 012032 https://doi.org/10.1088/1755-1315/950/1/012032.
Zhang, W., Qi, J., Wan, P., Wang, H., Xie, D., Wang, X., Yan, G., 2016. An easy-to-use airborne LiDAR data filtering method based on cloth simulation. Remote Sens. 8, 501. https://doi.org/10.3390/rs8060501.
Zhang, D., Liu, J., Ni, W., Sun, G., Zhang, Z., Liu, Q., Wang, Q., 2019. Estimation of forest leaf area index using height and canopy cover information extracted from unmanned aerial vehicle stereo imagery. In: IEEE J. Sel. Top. Appl. Earth Observations Remote Sensing, 12, pp. 471–481. https://doi.org/10.1109/JSTARS.2019.2891519.
Zhang, F., Tian, X., Zhang, H., Jiang, M., 2022. Estimation of aboveground carbon density of forests using deep learning and multisource remote sensing. Remote Sens. 14, 3022. https://doi.org/10.3390/rs14133022.